See B0287 2/6/85 PA2# - 743 1

Attachment-1

EXPECTED NUCLEAR WASTE REPOSITORY NEAR-FIELD SEE B0287 2/6/85

PERFORMANCE IN THREE SALT BASINS

Part I: Thermal Conditions

E. G. McNulty

February, 1984

8502270067 850206
PDR WMRES EXIORNL
B-0287 PDR

1 THERMAL CONDITIONS

Thermal analyses using site-specific thermal data provided time-dependent boundary temperatures for the waste package assessments and radial temperature profiles for the brine migration calculations. These analyses showed that Richton Dome, Gibson Dome, and Palo Duro salt basins will have significant differences in their expected near-field thermal performance. Richton Dome had much higher temperatures predicted than the other two sites because of the higher ambient in situ temperature and apparently lower thermal conductivity of the domal salt. Gibson Dome had slightly higher temperatures calculated than Palo Duro. Only commercial high-level waste (CHLW) and spent fuel from a pressurize boiler reactor (SFPWR) were considered. This section presents a benchmark of the analytical code TEMPV5 with temperatures calculated by Westinghouse (1983), defines the thermal data base, and presents the results of analyses using two emplacement schemes. One emplacement scheme assumes instantaneous emplacement of an infinite number of waste packages. The other scheme assumes sequential emplacement of a finite number of waste packages. Comparisons of the two emplacement schemes show that sequential emplacement yields temperatures only slightly lower than those found in an infinite array.

1.1 BENCHMARK OF TEMPV5

The TEMPV5 analytical code was used to make the thermal calculations. The TEMPV5 code is a much improved version of FLLSSM code (Kaiser, 1980). The temperatures calculated by the TEMPV5 code were compared to those published by Westinghouse (1983b, pp. 59-60) for tunnel and package spacings given in Table 1-1. Figure 1-1 gives the relationship between thermal conductivity and temperature. Figure 1-2 shows that the TEMPV5 code gives higher temperatures than those calculated with the finite element code WECAN by Westinghouse (1983b) for both CHLW and SF package designs. Table 1-2 summarizes the temperatures given in Figure 1-2.

The TEMPV5 code models individual waste packages as finite line sources in a homogeneous, isotropic, and infinite medium. The code uses linear superposition of temperature contributions from individual finite-line sources to calculate the temperature at a point. The code accounts for most of the

nonlinearity associated with the dependence of thermal properties on temperature through a transformation technique (Carslaw and Jaeger, 1959, pp. 10-11). The transformation technique also uses linear superposition to calculate contributions from surrounding heat sources to the temperature at a point. In addition, the code can consider the decay in heat generation for four types of nuclear waste, including CHLW and SFPWR. Finally, the TEMPV5 code can model the repository as an infinite or finite array of line sources.

The partial differential equation for heat conduction in an isotropic material is

$$\sum_{i=1}^{3} \partial(k\ \partial T/\partial x_i)/\partial x_i = \rho c\ \partial T/\partial t \qquad (1\text{-}1)$$

where

- T = temperature
- x_i = three principal coordinate directions
- t = time
- k = thermal conductivity
- ρ = density
- c = heat capacity

For constant thermal properties, that is, those which are independent of temperature and position, Equation 1-2 yields the temperature change at a point x_i' due to a continuous finite-line source:

$$\Delta T = \int_{-L}^{L} \int_{0}^{t} A(x_3', t')G\ (x_1-x_1', x_2-x_2', x_3-x_3', t-t')\ dt'dx_3' \qquad (1\text{-}2)$$

where

A = heat release rate per unit length for a source located at x_1' and x_2'.

L = half-length of line source whose midheight is $x_3' = 0$.

G = temperature function for heat source instantaneously generated at point x_i'.

$$= (\alpha/k)\ (4\pi\alpha(t-t'))^{-3/2} \exp\left(-\left((x_1-x_1')^2 + (x_2-x_2')^2 + (x_3-x_3')^2\right)/\ 4\alpha(t-t')\ \right) \tag{1-3}$$

and α = $k/\rho c$ = thermal diffusivity

t' = variable of integration.

The TEMPV5 codes assumes that the heat source remains constant with respect to x_3' but decreases with t'. Therefore,

$$A = q(t)/2L \tag{1-4}$$

where

$q(t)$ = total heat release rate of the line source

If thermal conductivity varies with temperature but remains independent of position, Equation 1-1 can be transformed into a linear form by defining a new function Φ

$$\Phi = \int_{T_o}^{T} k\ dT \tag{1-5}$$

where T_o is the ambient initial temperature of the infinite medium. In terms of Φ Equation 1 becomes

$$\sum_{i=1}^{3} \partial^2\Phi/\partial x_i^2 = \frac{1}{\alpha}\partial\Phi/\partial t \tag{1-6}$$

If thermal diffusivity α is constant, linear superposition applies to Equation 1-6.

The TEMPV5 codes allows thermal conductivity to vary spatially within the salt as a function of temperature through the use of the chain rule with Equation 1-5 in the following form

$$\frac{\partial \Phi}{\partial x_i} = k \frac{\partial T}{\partial x_i} \tag{1-7}$$

Substitution of Equation 1-7 into the left hand side of Equation 1-6 yields

$$\frac{1}{\alpha} \partial\Phi/\partial t = \frac{\partial}{\partial x_i} \left(k \frac{\partial T}{\partial x_i}\right) \tag{1-8a}$$

$$= \frac{\partial k}{\partial x_i} \frac{\partial T}{\partial x_i} + k \frac{\partial^2 T}{\partial x_i^2} \tag{1-8b}$$

$$= \frac{\partial k}{\partial T} \left(\frac{\partial T}{\partial x_i}\right)^2 + k \frac{\partial^2 T}{\partial x_i^2} \tag{1-8c}$$

where the first term of the right hand side clearly shows the spatial variation of thermal conductivity as a function of temperature.

The analytical code TEMPV5 avoids difficulties associated with numerical models such as WECAN (Westinghouse, 1983b, pg. I91), a finite element code. For example, most numerical codes model the waste package as a rectangular parallelepiped rather than as a cylinder. Inaccurate near field temperatures result from a rectangular configuration of the waste package. In addition, numerical codes require considerable user sophistication. Temperatures near the waste package may be underpredicted if the finite element grid is too coarse. Not only does the grading of the finite element mesh have a crucial effect on the calculated temperatures, but also on the allowable time step. Smaller nodal spacings require smaller time steps.

In contrast, the TEMPV5 code is much easier to use than most numerical codes because it does not require the analyst to consider the errors caused by too coarse a mesh or too large a time step. In addition, the TEMPV5 code is less expensive to use than a numerical code. The simplicity and efficiency of TEMPV5 in data manipulation and calculation reduces the time required by people and computer to analyze a given problem. Finally, the uncertainty associated with material properties of the data base used in these analyses argues against the use of sophisticated numerical codes for the near-field thermal assessments.

1.2 DATA BASE

The data used in the thermal analyses consisted of site-specific thermal properties (Lagerdrost and Capps, 1983), waste package parameters (Westinghouse, 1983a, Tables 1-2 and 1-3), and baseline repository parameters (Stearns-Roger, 1983, Tables 5-1, 2, and 3).

Site-specific thermal data consisted of ambient in situ temperatures, thermal conductivities, specific heats, and salt densities. The ambient temperature establishes the initial temperature field upon which the heat generated by the emplaced waste is superimposed. Table 1-3 summarizes the ambient in situ temperatures for Palo Duro, Gibson Dome in the Paradox Basin, and Richton Dome. The geothermal gradient for the Palo Duro Basin varies areally in a range of 13 to 27 C/km-depth (Dutton 1980, p. 40). The geothermal gradient for Gibson Dome varies between about 10 to 30 C/km-depth (Sass et al, 1983, Fig. 1). The geothermal gradient for Richton Dome varies between about 26 and 32 C/km (Law, 1983, Pg. 13) for depths 300 to 3,400 meters.

Site-specific thermal conductivities of salt were obtained from Lagedrost and Capps (1983, Tables 14, 15, 16, 20, 21, 22, 23, 24 and 25) as shown in Figures 1-3, 4, and 5. Laboratory thermal conductivities were increased to compensate for reductions caused by the Pyroceram 9606 calibration standard and specimen disturbance. First, Figure 1-6 shows the correction required to bring the Lagedrost and Capps standard (1981) near the standard recommended by Touloukian et al (1970, Fig. 20). Second, Figure 1-7 (adapted from Loken et al, 1982, Fig. D.3) shows that the data by Lagedrost represented the lower bound of laboratory thermal conductivities of salt which were obtained from a survey of the literature. The conductivities reported by Lagedrost required a 40 percent increase to put the data curve near the middle of the range of possible values as shown in Figure 1-7. Thermal conductivities measured in the laboratory are generally substantially lower than actual field values as a result of disturbance caused by stress relief or sampling and specimen preparation. Wagner (1981, pg. 9) showed that a 20 percent increase in

laboratory thermal conductivities was required to match numerical predictions with actual in situ test results at Avery Island. Duffey (1980, Figs. 3, 20, pp. 7, 59) found that thermal conductivities derived from laboratory tests had to be increased 100 percent to match results of bench scale tests on New Mexico salt. Hence, the 40 percent increase for laboratory thermal conductivities is justified and was used to increase the thermal conductivities for each of the three salt sites.

Figures 1-3, 1-4, and 1-5 present exponential forms for the thermal conductivities. The TEMPV5 code requires that the thermal conductivities be represented by an equation of the form

$$K = A/T + B, \qquad (1\text{-}9)$$

where A and B are the slope and intercept, respectively, of the linear regression of the fitted data. Consequently, conversions were made for the exponential relationships of each site. Figures 1-8, 9, and 10 show that there is excellent agreement between the TEMPV5 and exponential representations of the thermal conductivities. The 40 percent increase in thermal conductivities has been included.

A comparison of thermal conductivities of the three salt sites in Figure 11 suggests that the thermal conductivities of Richton domal salt is significantly different from those of Palo Duro and Gibson Dome. The salt specimens from Richton may have had more anhydrite than those from the other two sites. Anhydrite has a lower thermal conductivity than pure salt (Sweet and McCreight, 1980, Fig. 5). Consequently, larger amounts of anhydrite or similar impurities in salt specimens would lower the measured thermal conductivities. However, anhydrite may also increase the sensitivity of the salt specimens to disturbance caused by stress relief. Reductions in measured salt thermal conductivity caused by fractures opening as a result of stress relief may be larger than reductions caused by the lower thermal conductivity of impurities such as anhydrite.

Nominal variations in specific heat of salt (Lagerdrost and Capps, 1983, Tables 15, 21, and 24) and salt density (Lagerdrost and Capps, 1983, Tables 16, 22, and 25) were observed among the three sites. Consequently, averages of the specific heat and density over the three sites could be used in the

PA-2 V
DC8

thermal analyses with TEMPV5. The diffusivities used by TEMPV5 were calculated from these averages. Because diffusivity does not vary with temperature in TEMPV5, represented values were estimated to be 2.4E-6 and 2.6E-6 m^2/sec for temperature ranges expected for CHLW and SFPWR waste, respectively. Figure 1-12 shows that expected changes in diffusivity as a result of temperature variations will have a small effect on temperatures calculated by TEMPV5.

Waste package parameters (outer diameter of overpack and effective length of waste package) were taken from Westinghouse (1983a) for Alternate II Designs of SFPWR and CHLW. These two designs will be simply referred to as SFPWR and CHLW. Table 1-4 gives the TEMPV5 heat release rate with time for these two waste forms.

Baseline repository parameters (areal thermal loading, tunnel and package spacings, and room development rates) were given by Stearns-Roger (1983, Tables 5-1, 2, and 3). Table 1-5 summarizes the relevant repository data. Table 1-6 summarizes the corresponding room development rates for SFPWR and CHLW.

1.3 THERMAL ANALYSES AND RESULTS

Site-specific thermal analyses were made for each salt formation assuming that the waste had been emplaced in an infinite array. Analyses were based on the data found in Table 1-5. These analyses assessed the effect of site-specific thermal data on the surface temperatures of the waste package. In addition, analyses were made with thermal data for Palo Duro to establish the effect of sequential emplacement on the surface temperatures of the waste package.

Site-specific temperatures calculated for CHLW and SFPWR waste forms using an infinite array configuration are shown in Figures 1-13, 14, 15, and 16. Tables 1-7, 8, 9, and 10 summarize temperatures as a function of time for each salt site. As shown in Table 1-11, Richton Dome has the highest peak temperatures for both CHLW and SFPWR waste.

The infinite array calculation leads to an early peak of the maximum temperatures. Sequential loading analyses were made to evaluate the conservatism, if any, in the infinite array predictions of the surface

temperatures on the waste package. Algorithmic limitations in TEMPV5 for sequential loading analyses required that the repository layout given in Figure 1-17 be used, that temperatures be calculated separately for each waste form, and that the emplacement rates given in Table 1-6 be changed slightly to account for differences in the repository layout. In spite of these adjustments, very few differences were found among temperatures calculated with a sequential loading in a finite array and those calculated with an instantaneously emplaced infinite array. Figures 1-18 and I9 compare sequential emplacement temperatures with those of the infinite array on an absolute time scale. Figures 1-20 and 21 show that back-shifting all times of emplacement to zero years makes the infinite array and sequential emplacement temperatures almost coincide. The comparison in Figures 19 1-and 20 shows that the infinite array temperatures after 100 years are slightly higher by about 10 C for CHLW and 15 C for SFPWR.

1.4 CONCLUSIONS AND RECOMMENDATIONS

The accuracy of temperatures calculated for each salt site depends on the accuracy of TEMPV5, reliability of the site-specific thermal data, and appropriateness of the infinite array configuration of the waste packages.

The TEMPV5 code predicts temperatures with sufficient accuracy for several reasons. First, the code accounts for the temperature dependence of thermal conductivity. Second, nonsalt materials around the repository horizon could be ignored because only near-field temperatures were calculated. Third, the TEMPV5 code provided modeling alternatives that were not available with other heat transfer codes. Finally, the TEMPV5 code provided temperatures which were significantly higher than those given by Westinghouse (1983b). Consequently, not only were the TEMPV5 temperatures more conservative than those of Westinghouse (1983b), but probably more accurate because Westinghouse (1983b) modeled the waste package with a rectangular cross section. However, the TEMPV5 code should be benchmarked with a numerical code which models the waste package as a cylinder to define at what distances from finite-line source the TEMPV5 code gives accurate temperatures.

Next, the accuracy of the temperatures computed for each salt site depended on the reliability of the ambient in situ temperatures and thermal

conductivities. First, the ambient in situ temperature varied areally at Palo Duro by 3 C (Dutton, 1980, p. 40). A similar variation could be expected in the bedded salt at Gibson Dome because of similar variations in geothermal gradient. The uncertainty in the ambient in situ temperatures at Richton are less than those at Palo Duro and Gibson Dome because of the smaller variation in the geothermal gradient. Second, the differences observed among the thermal conductivities of the three sites may have had as much to do with the site-specific sensitivity of salt specimens to stress relief as the differences had to do with the thermal conductivity of impurities such as anhydrite. The effect of stress relief needs to be quantified to establish the accuracy of laboratory thermal conductivities.

Finally, Figures 1-18, 19, 20, and 21 show that the infinite array solution gives nearly the same temperatures as those computed assuming sequential emplacement. However, the TEMPV5 code should be modified to give each region of the repository the option to have any type of waste, number of tunnels, number of packages, and package spacing. These modifications would improve assessment of the impact of sequential emplacement on the near-field temperatures.

REFERENCES

Capps, W. and J. F. Lagedrost, September, 1981a. Thermal Property and Density Measurements of Samples Taken from Drilling Cores from Potential Geologic Media, Interim Reports (12) on Materials from the Gibson Salt Dome-1 Paradox Basin, Utah, prepared by Fiber Materials Inc., Biddeford, MN, for Office of Nuclear Waste Isolation, Battelle Memorial Institute, Columbus, OH.

Capps, W. and J. F. Lagedrost, September, 1981b. Thermal and Density Measurements of Samples Taken from Drilling Cores from Potential Geologic Media Interim Reports (4) on Materials from the Richton Salt Dome, MRIG-9, Mississippi, prepared by Fiber Materials Inc., Biddeford, ME, for Office of Nuclear Waste Isolation, Battelle Memorial Institute, Columbus, OH.

Carslaw, H. S. and J. C. Jaeger, 1959. Conduction of Heat in Solids, 2nd ed., Clarendon Press, 1959.

Duffey, T. A., 1980. Final Report--The Salt Block I Test: Experimental Details and Comparison with Theory, SAND79-7050, Los Alamos Technical Associates, Inc., February.

Dutton, S. P., 1980. Depositional Systems and Hydrocarbon Resource Potential of the Pennsylvania System Palo Duro and Dalhart Basins, Texas Panhandle, Geological Circular 80-8, Bureau of Economic Geology, The University of Texas at Austin, TX.

Kaiser Engineers, Inc., March 1980. Finite-Length Line Source Superposition Model (FLLSSM), ONWI-94, prepared for Office of Nuclear Waste Isolation, Battelle Memorial Institute, Columbus, OH.

Lagedrost, J. F., September, 1980a. Thermal Property and Density Measurements of Samples Taken from Drilling Cores from Potential Geologic Media, Interim Reports (4) on Materials from the Vacherie Dome, Louisiana, prepared by Fiber Materials Inc., Biddeford, ME, for the Office of Nuclear Waste Isolation, Battelle Memorial Institute, Columbus, OH.

Lagedrost, J. F., September, 1980b. Thermal Property and Density Measurements of Samples Taken from Drilling Cores From Potential Geologic Media, Interim Reports (4) on Materials from Salt Valley DOE-3, No. 13827A, prepred by Fiber Materials Inc., Biddeford, ME, for the Office of Nuclear Waste Isolation, Battelle Memorial Institute, Columbus, OH.

Lagedrost, J. F., September, 1980c. Thermal Property and Density Measurements of Samples Taken from Drilling Cores from Potential Geologic Media, Interim Reports (6) on Materials from the Richton Salt Dome, MRIG-9, Mississippi, prepared by Fiber Materials Inc., Biddeford, ME, for the Office of Nuclear Waste Isolation, Battelle Memorial Institute, Columbus, OH.

Lagedrost, J. F., March, 1980d. Thermal Property and Density Measurements of Samples Taken from Drilling Cores from Essential Geologic Media, Interim Reports (8) on Materials from Randall and Swisher Counties, Texas, prepared by Fiber Materials Inc., Biddeford, ME, for the Office of Nuclear Waste Isolation, Battelle Memorial Institute, Columbus, OH.

Lagedrost, J. F., July, 1981. Thermal Property and Density Measurements of Samples Taken from Drilling Cores from Potential Geologic Media, Interim Reports (4) on Materials from the Richton Salt Dome, MRIG-9, Mississippi, prepared by Fiber Materials, Inc., Biddeford, ME, for the Office of Nuclear Waste Isolation, Battelle Memorial Institute, Columbus, OH.

Lagedrost, J. F. and W. Capps, December, 1983. Thermal Property and Density Measurements of Samples Taken From Drilling Cores From Potential Geologic Media, BMI/ONWI-522, prepared by Fiber Materials, Inc., for the Office of Nuclear Waste Isolation, Battelle Memorial Institute, Columbus, OH.

Law Engineering Testing Company, 1983. Geothermal Studies of Seven Interior Salt Domes, ONWI-289, prepared for Office of Nuclear Waste Isolation, Battelle Memorial Institute, Columbus, OH.

Loken, M. C., Cullahan, G. D., Svalstad, D. K., December 1982, Thermo-mechanical Analyses of Conceptual Repository Designs for the Paradox and Permian Basins, RE/SPEC, Inc., Rapid City, SD, RSI-0204, prepared for the Office of Nuclear Waste Isolation, Battelle Memorial Institute, Columbus, OH, ONWI-(unpublished).

Sass, J. H., A. H. Lachenbruch, and E. P. Smith, 1983. Thermal Data from Well GD-1, Gibson Dome, Paradox Valley, Utah, U.S. Geological Survey Open-File Report 83-476.

Stearns-Roger, 1983. Engineering Factors and Costs for NWTS Repository Site Selection Deaf Smith/Swisher Counties, Texas-May 1983, ONWI-???, prepared for Office of Nuclear Waste Isolation, Battelle Memorial Institute, Columbus, OH.

Sweet, J. N. and J. E. McCreight, 1980. Thermal Properties Measurement on Rocksalt Samples from the Site of the Proposed Waste Isolation Pilot Plant, SAND 80-0799, Sandia National Laboratories.

Touloukian, Y. S., R. W. Powell, C. Y. Ho, and P. G. Klemens, 1970. "Thermal Conductivity: Nonmetallic Solids", Thermal Properties of Matter, Volume 2, IFI/PLENUM, New York-Washington, Figure 20.

Wagner, R. A., August 1981. Comparison and Evaluation of Field and Numerical Results from the Site Heater Test at Avery Island, ONWI-300, Office of Nuclear Waste Isolation, Battelle Memorial Institute, Columbus, OH.

Westinghouse Electric Corporation, 1983a. Engineering Waste Package Conceptual Design: Defense High-Level Waste (Form 1), Commercial HighLevel Waste (Form 1), and Spent Fuel (Form 2) Disposal in Salt, ONWI-438, prepared for Office of Nuclear Waste Isolation, Battelle Memorial Institute, Columbus, OH.

Westinghouse Electric Corp., 1983b. Waste Package Reference Conceptual Designs for a Repository in Salt, WTSD-TME-001, ONWI- , Battelle Project Management Division, Office of Nuclear Waste Isolation, Columbus, OH.

PA2-4
DC-14

Table 1-1. Tunnel and Package Spacings for Benchmark Comparison of TEMPV5 with Westinghouse 1983b

Waste Form	Areal Loading, W/m^2	Overpack* Outer Diameter	P_L*	S*	WP_L*
SF	14.83	0.845	22.14	20.1	3.66
CHLW	15	0.763	24.17	22.2	3.68

* Dimensions in meters (m).

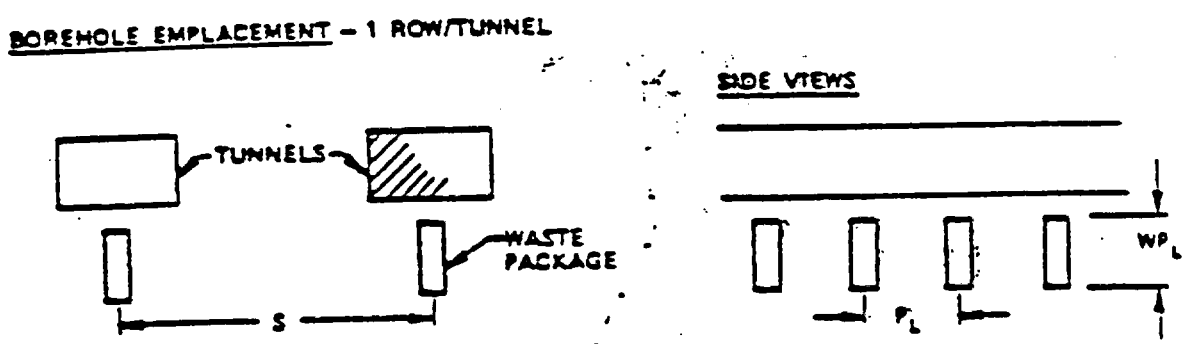

FA 2-4
DC-15

Table 1-2. Benchmark Comparison of TEMPV5 and Westinghouse 1983b Temperatures at Salt-Overpack Interface

Time (years)	Temperature, C			
	CHLW		SFPWR	
	Westinghouse	TEMPV5	Westinghouse	TEMPV5
0.1	200	271.1	147	174.8
0.5	227	298.8	163	190.0
1	229	301.7	169	193.1
2	230	300.8	172	195.4
5	228	290.3	178	197.5
7.5	222		177	
10	215	267.0	172	197.5
20	197	222.2	165	191.8
30	173	187.4	155	183.3
50	126	143.0	136	167.0
70	100	118.9		153.9
100	89	100.8	117	139.6
200	75	82.3	95	116.2
400	66	69.3		103.5
500		64.9	83	100.9
700	62	58.5		96.6
1000	59	52.5	78	90.6
2000		44.4		73.9
5000		37.0		50.7
7000		34.1		43.8
10000		34.0		36.4

PA 2-4
DC-4

Table 1-3. Ambient In Situ Temperature, T_o, For Three Salt Sites

	Ambient In Situ Temperature, C	Reference
Palo Duro	28.2	*Dutton, S. P. (1980)
Gibson Dome	31.0	Loken et al (1982, Fig. 4.10)
Richton Dome	48.3	Law (1983, pg. 39)

* Assuming surface temperature of 16 C and geothermal gradient of 20 C/km depth.

Table 1-4. Heat Release Rates for CHLW (9.1 MTIHM)* and SFPWR (4.614 MTIHM) in TEMPV5

(After Discharge years)	Heat Release Rates, watts	
	CHLW	SFPWR
10	9503	5417
30	5016	3386
50	2909	2483
100	1141	1400
300	418.8	555.7
500	214.2	420.9
1000	40.12	247.2
3000	4.94 E-02	30.03
5000	6.07 E-05	3.647
10000	0.0	1.875 E-02
30000	0.0	0.0

* MTIHM = metric tons heavy metal before irradiation.

Table 1-5. Tunnel and Package Quantities

Waste[a] Form	Areal Loading[b], W/M^2	Waste Packages[b] per Room	Number[b] of Waste Packages	Overpack[a] Outer Diameter*	P_L[b]*	S[b]*	WP_L[a]*
SFPWR	15	9	7,899	0.835	18.3	20.1	3.85
CHLW	30	13	3,673	0.890	12.2	26.2	3.68

* Dimensions in meters (m).
(a) Westinghouse (1983a)
(b) Stearns - Roger, 1983.

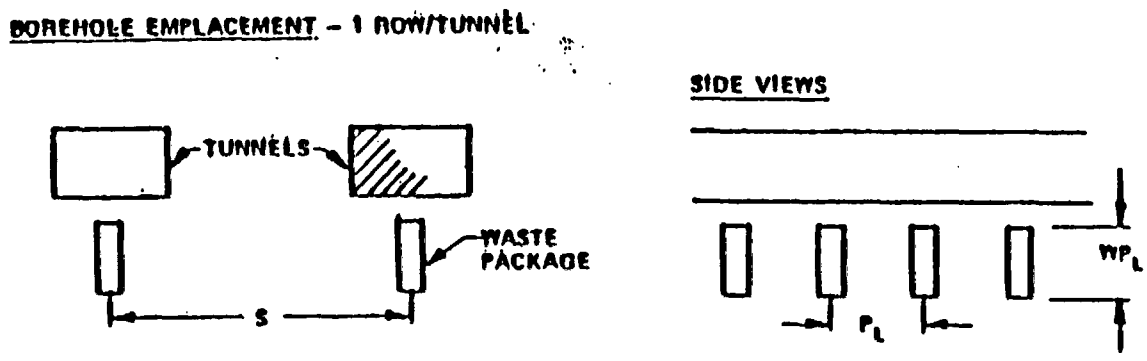

Table 1-6. Development Rates for Waste Storage Rooms (Stearns-Roger, 1983)

Year*	Number of Rooms Required to Receive Waste	
	SFPWR	CHLW
1	21	7
2	21	7
3	21	7
4	21	7
5	21	7
6	37	12
7	37	12
8	37	12
9	37	12
10	37	12
11	37	12
12	37	12
13	37	12
14	37	12
15	37	12
16	37	12
17	37	12
18	37	12
19	37	12
20	37	12
21	37	12
22	37	12
23	37	12
24	37	12
25	37	12
26	33	8
Totals	878	283

* Starting with the first year of emplacement.

Table 1-7. Infinite Array CHLW Temperature Versus Time (TEMPV5) At Salt-Overpack Interface Assuming Equal In Situ T_o for Three Salt Sites

Time (years)	Temperature, C		
	Palo Duro, T_o = 28.2 C	Gibson Dome, T_o = 31 C	Richton Dome, T_o = 48.3 C
0.1	174.5	185.2	228.4
0.2	185.4	197.0	240.7
0.5	197.2	210.0	253.8
1	204.9	218.4	262.2
2	212.2	226.5	270.2
5	219.8	234.9	278.5
10	217.4	232.3	276.0
20	198.2	211.2	255.0
50	145.3	153.7	194.7
100	108.4	114.4	150.7
200	89.2	94.2	126.9
500	69.8	73.9	102.6
1000	54.2	57.8	82.8
2000	42.6	45.8	68.2
5000	30.8	33.8	54.2
10000	28.2	31.0	48.3

Table 1-8. Infinite Array CHLW Temperature Versus Time (TEMPV5) At Salt-Overpack Interface Assuming Equal In Situ T_o for Three Salt Sites

Time (years)	Temperature, Celsius		
	Palo Duro, T_o = 28.2 C	Gibson Dome, T_o = 28.2 C	Richton Dome, T_o = 28.2 C
0.1	174.5	180.8	202.8
0.2	185.4	192.6	214.7
0.5	197.2	205.3	227.5
1	204.9	213.7	235.7
2	212.2	221.7	243.6
5	219.8	230.0	251.6
10	217.4	227.5	249.2
20	198.2	206.5	228.7
50	145.3	149.6	170.0
100	108.4	110.8	127.1
200	89.2	90.8	104.1
500	69.8	70.7	80.6
1000	54.2	54.7	61.4
2000	42.6	42.9	47.2
5000	30.8	31.0	33.6
10000	28.2	28.2	28.2

DA 7-4
DC-2?

Table 1-9. Infinite Array SFPWR Temperature Versus Time (TEMPV5) At Salt-Overpack Interface for Three Salt Sites

Time (years)	Temperature, C		
	Palo Duro, T_o = 28.2 C	Gibson Dome, T_o = 31 C	Richton Dome, T_o = 48.3 C
0.1	105.5	111.2	146.9
0.2	110.1	116.1	152.5
0.5	113.8	120.1	157.2
1	116.3	122.7	160.1
2	118.7	125.2	163.0
5	121.9	128.6	166.9
10	124.0	130.8	169.4
20	123.2	130.0	168.5
50	112.2	118.4	155.2
100	97.5	102.9	137.2
200	83.8	88.5	120.1
500	74.1	78.4	108.1
1000	67.4	71.4	99.7
2000	55.7	59.4	85.1
5000	38.1	41.3	63.4
10000	28.2	31.0	48.8

Table 1-10. Infinite Array SFPWR Temperature Versus Time (TEMPVS) At Salt-Overpack Interface Assuming Equal T_o for Three Salt Sites

Time (years)	Temperature, C		
	Palo Duro, T_o = 28.2 C	Gibson Dome, T_o = 28.2 C	Richton Dome, T_o = 28.2 C
0.1	105.5	107.6	123.5
0.2	110.1	112.5	129.0
0.5	113.8	116.5	133.5
1	116.3	119.0	136.3
2	118.7	121.5	139.1
5	121.9	124.9	142.9
10	124.0	127.1	145.3
20	123.2	126.3	144.4
50	112.2	114.7	131.5
100	97.5	99.4	114.1
200	83.8	85.1	97.5
500	74.1	75.2	85.9
1000	67.4	68.2	77.7
2000	55.7	56.3	63.6
5000	38.1	38.4	42.4
10000	28.2	31.0	28.2

Table 1-11. Peak Temperatures (TEMPV5) at Each Salt Site for Infinite Array Analyses Using Ambient In Situ Temperatures, T_o

	Time (years)	Peak Temperature, C		
		Palo Duro, T_o = 28.2 C	Gibson Dome, T_o = 31 C	Richton Dome, T_o = 48.3 C
CHLW	5	220	235	279
SFPWR	10	124	131	169

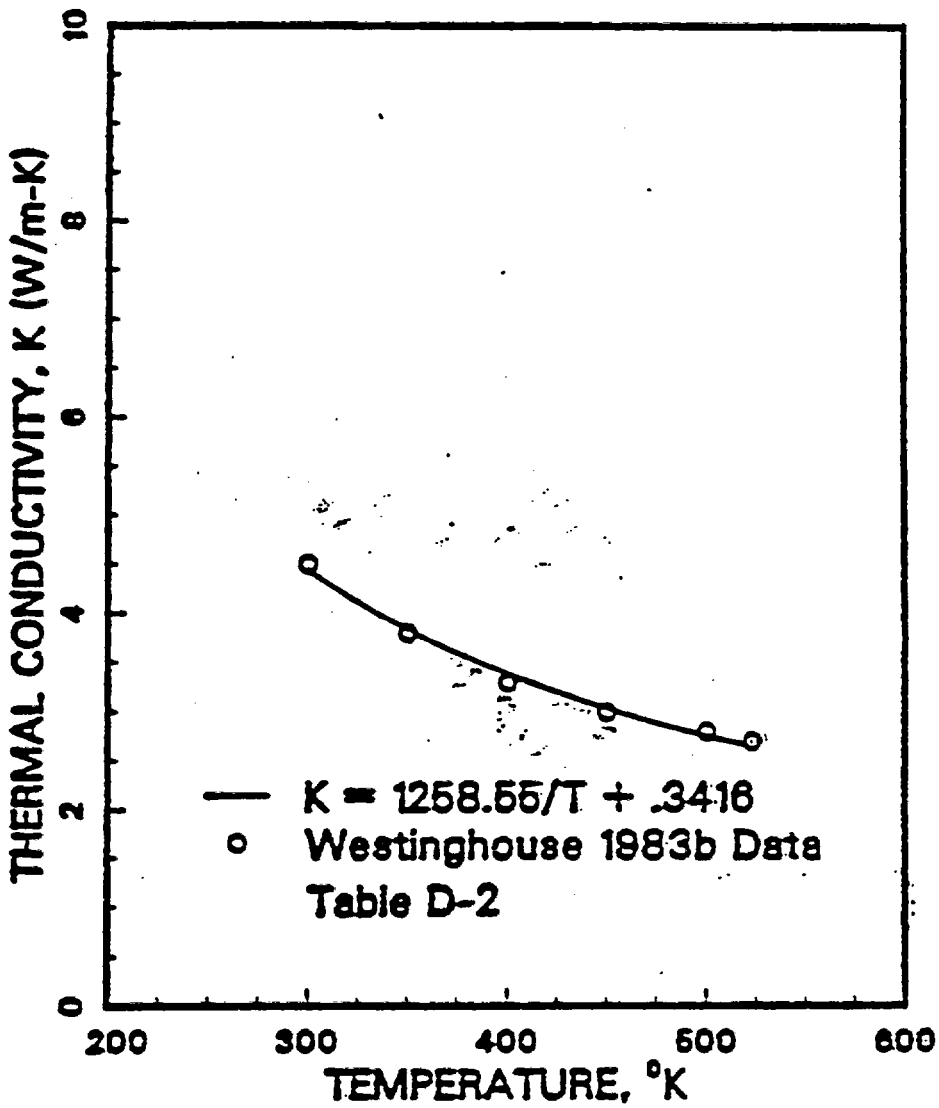

Figure 1-1

Comparison of K = A/T + B form for TEMPV5 Thermal Conductivity with Raw Thermal Conductivities from Westinghouse 1983b
DATA SET WTSD.FOR, SD.EAGRAPH, 11/02/83 EGM

7+2-4
DC 27

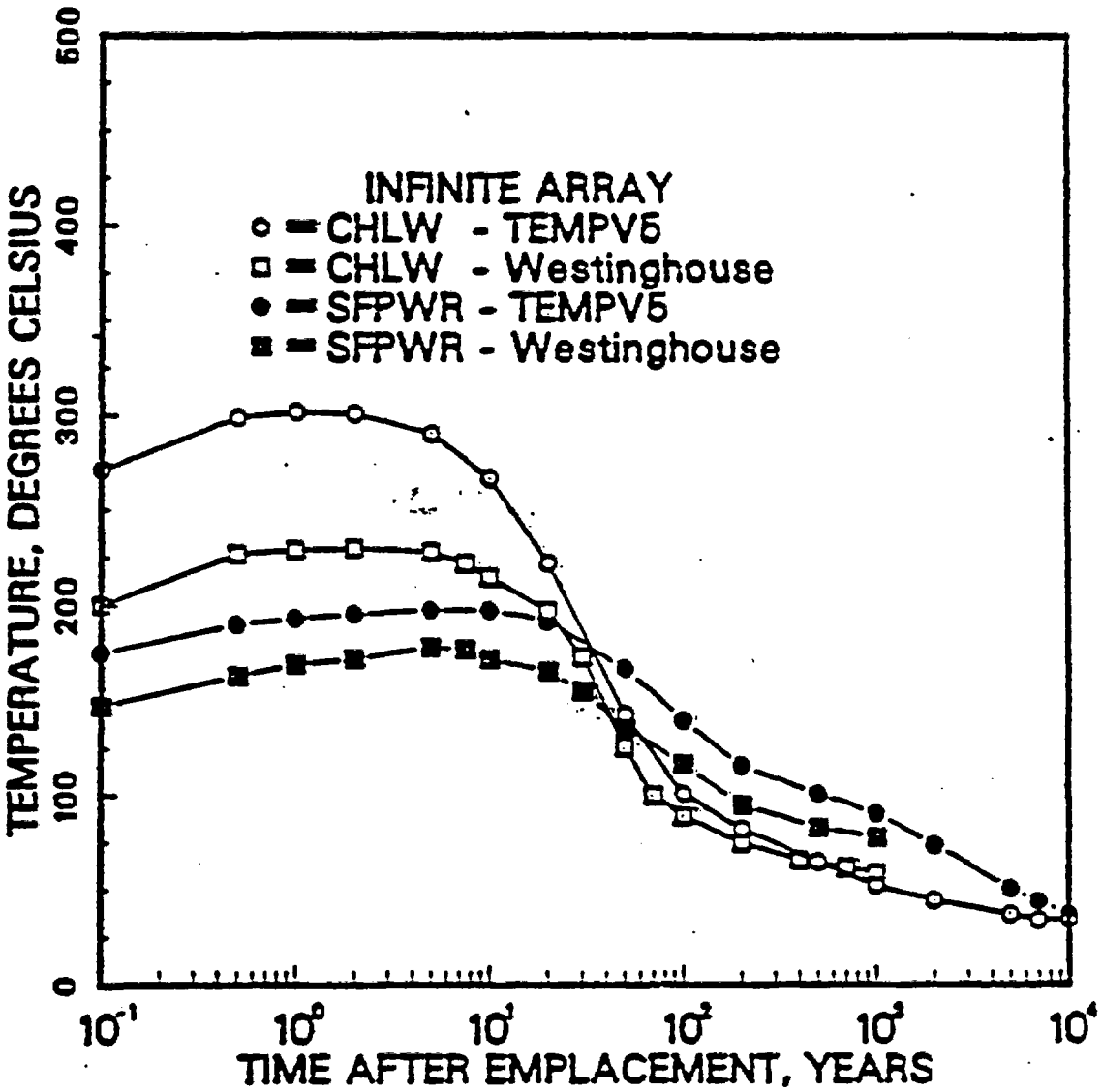

1-2

Benchmark Comparison of TEMPV5 with Westinghouse
1983b Results at Salt-Overpack Interface
DATA SET BENCH1.FOR, SD.EAGRAPH, EGM 1/03/84

PA 2 # DC-28

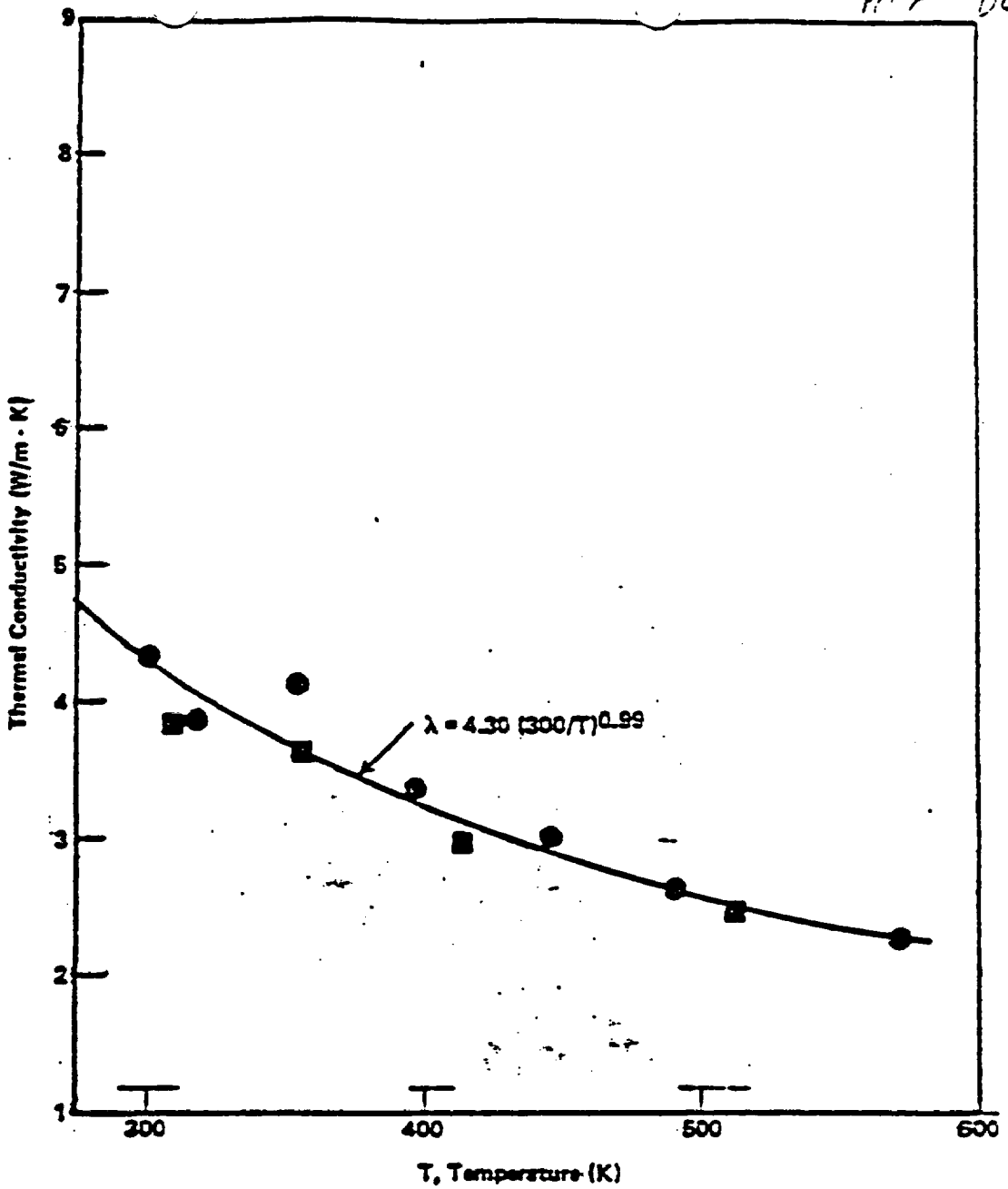

Key

● Borehole, Depth, Lithology

■ Rexwhite, 563 m, Lower San Andres Unit 4 Halite
Grabbe, 770 m, Lower San Andres Unit 4 Halite

Source: Data from Lagedrost (1980).

Figure 1-3
Thermal Conductivity of Palo Duro Halite From Unit 4 of the Lower San Andres Formation

~~Figure 2-7~~

1-3 Fig 3

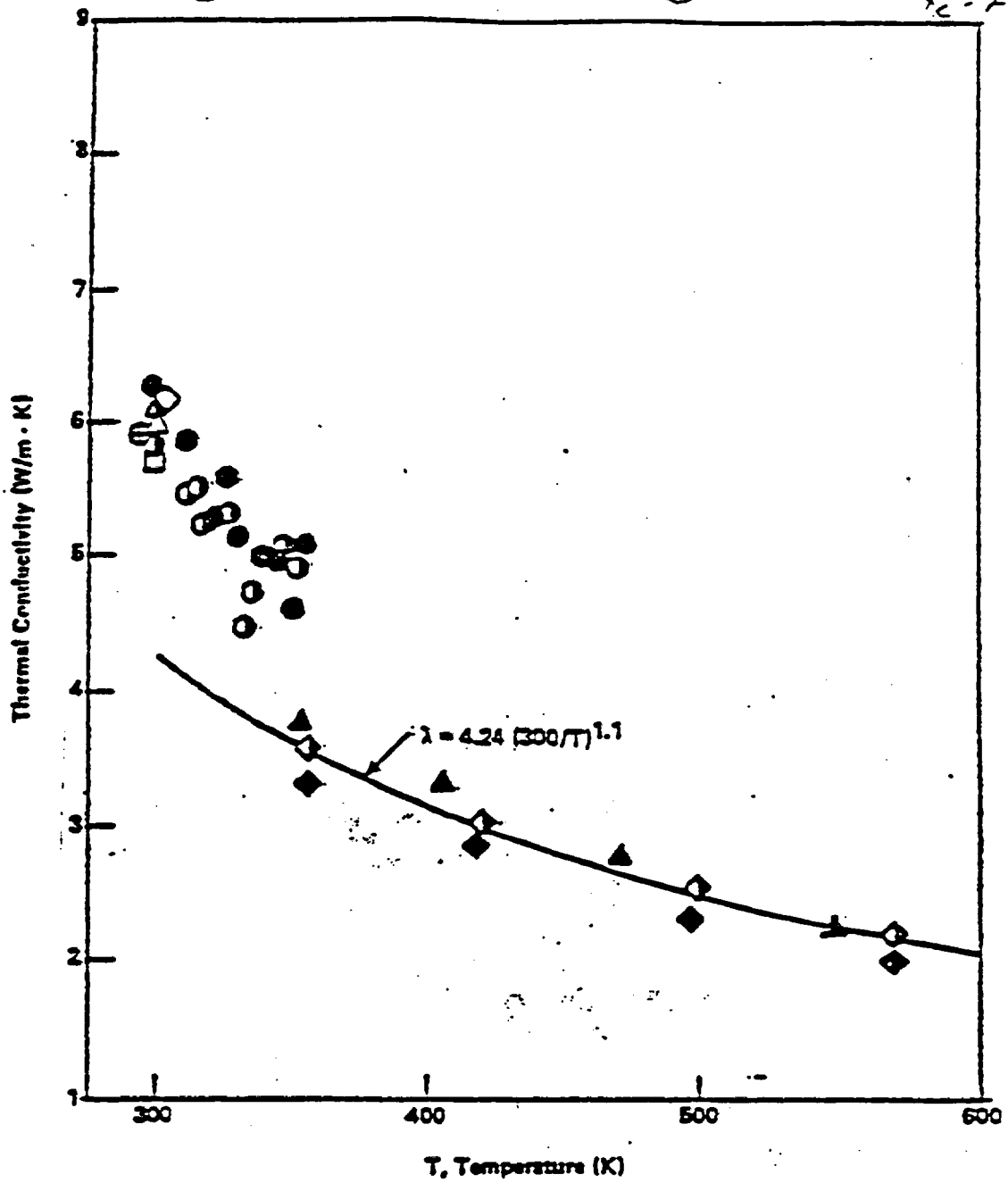

Key

Data From Capps & Lappdrant (1981)

- △ GD-1, 914 m, Paradox Unit 5 Halite With Anhydrite
- ◇ GD-1, 1048 m, Paradox Unit 7 Halite With Anhydrite
- ◆ GD-1, 1051 m, Paradox Anhydrite With Halite

Data From Sass et al. (1983)

- ● GD-1, 914 m, Paradox Unit 5 Halite (xy)[a]
- ◑ GD-1, 1180 m, Paradox Anhydrite With Halite (xy)
- ⊖ GD-1, 1310 m, Paradox Unit 16 Halite (xyz)
- □ GD-1, 914 m, Paradox Unit 5 Halite (xy)
- △ GD-1, 1066 m, Paradox Unit 8 Halite (xy)
- ▲ GD-1, 1066 m, Paradox Unit 8 Halite (xyz)
- ◇ GD-1, 1310 m, Paradox Unit 16 Halite (xy)

Note

(a) 'xy' indicates probe vertical to core axis.
'xyz' indicates probe horizontal to core axis.

Fig 1-4

Thermal Conductivity of Various Gibson Dome Halite Units of the Paradox Formation

Figure 2-10

Fig 1-4

P.4 2-4
DC-30

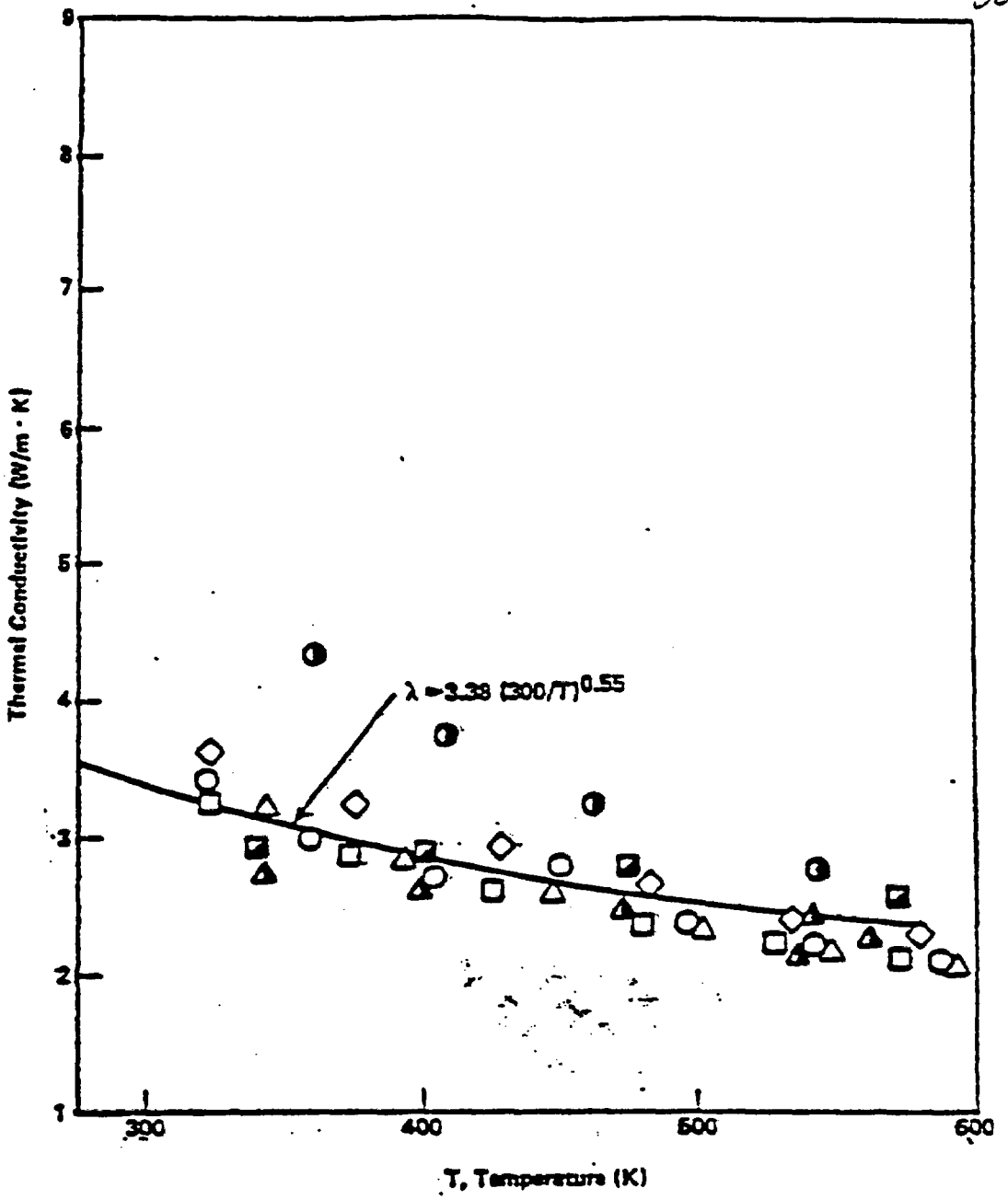

Source: Data points from Lagedrost (1980), Capps & Lagedrost (1981).

Key

Borehole, Depth	Borehole, Depth
MRIG-9, 243 m	MRIG-9, 305 m
MRIG-9, 262 m	MRIG-9, 378 m
MRIG-9, 294 m	MRIG-9, 384 m
MRIG-9, 325 m	

1-5

Thermal Conductivity of Richton Dome Halite

Figure 2-1

Fig 5

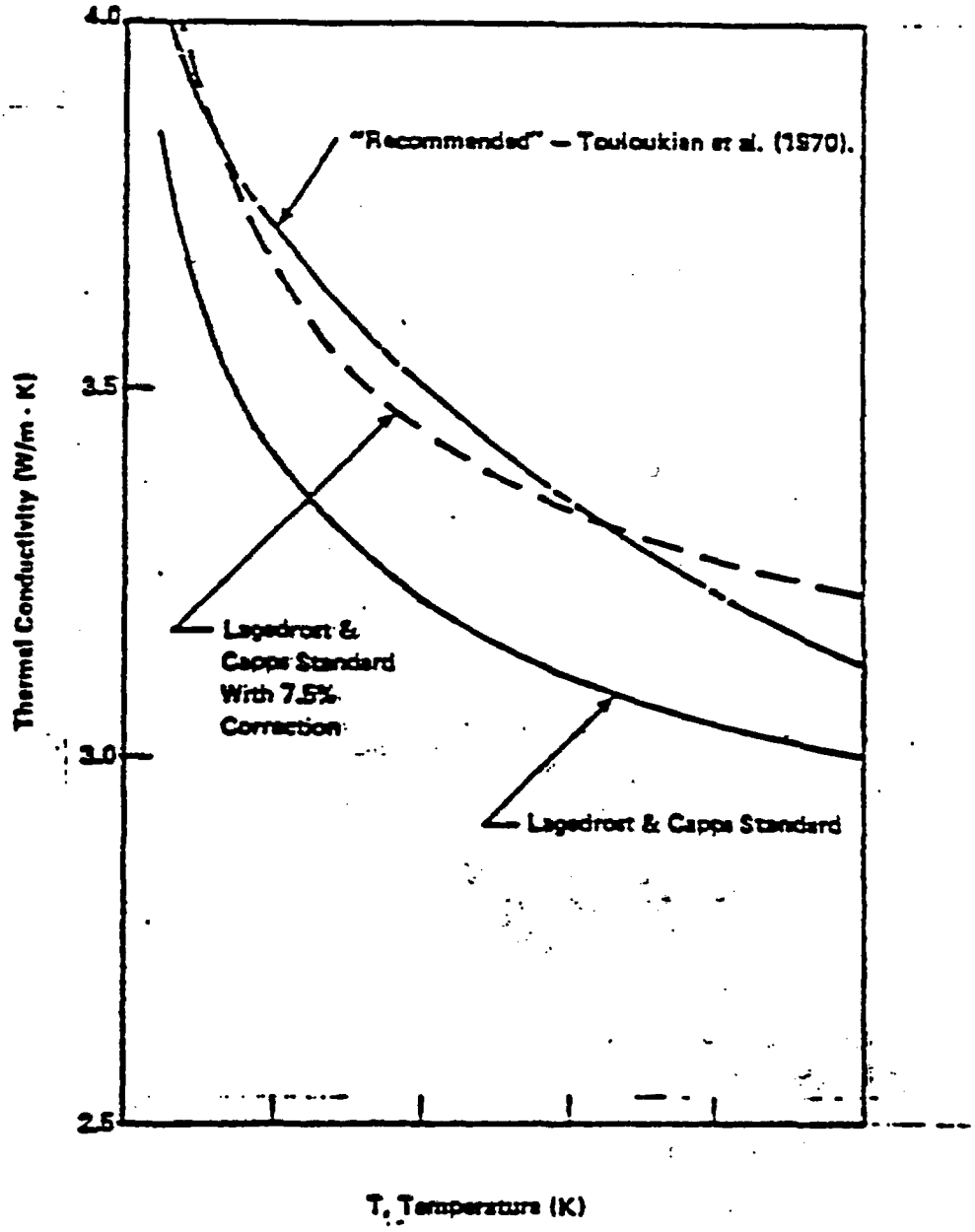

Key

——— Touloukian et al. (1970).

——— Lagedroot & Capps Standard (1983)

—·—·— Lagedroot & Capps Standard increased 7.5%

1-6 Thermal Conductivity Value of Pyroceram 9606

Figure 2-12

PA 2-4
DC-32

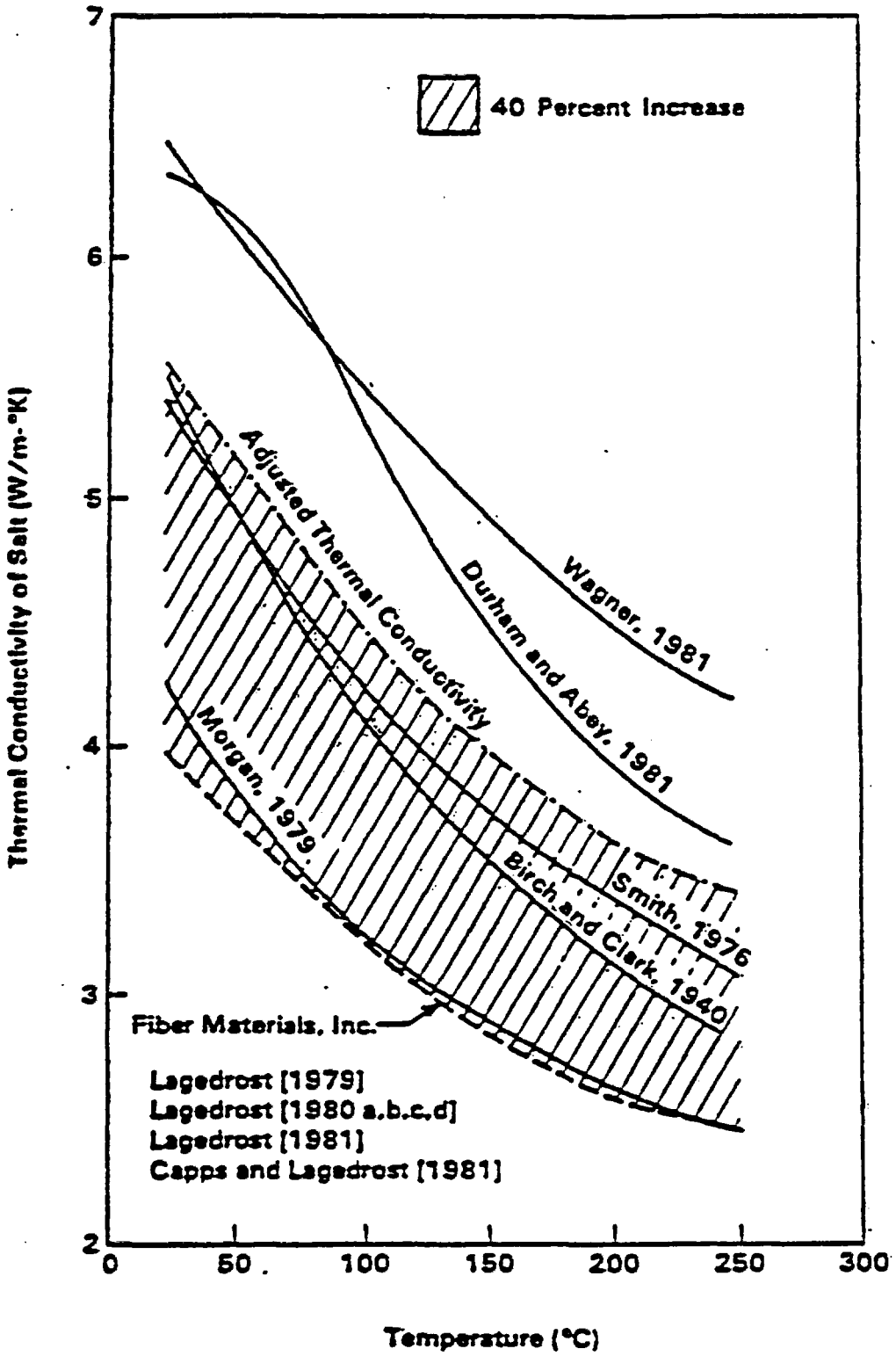

1-7

A DATA COMPILATION FOR THE THERMAL CONDUCTIVITY OF SALT AS DETERMINED BY LITERATURE REVIEW

(Adapted from Loken et al 1982)

Fig 1-7

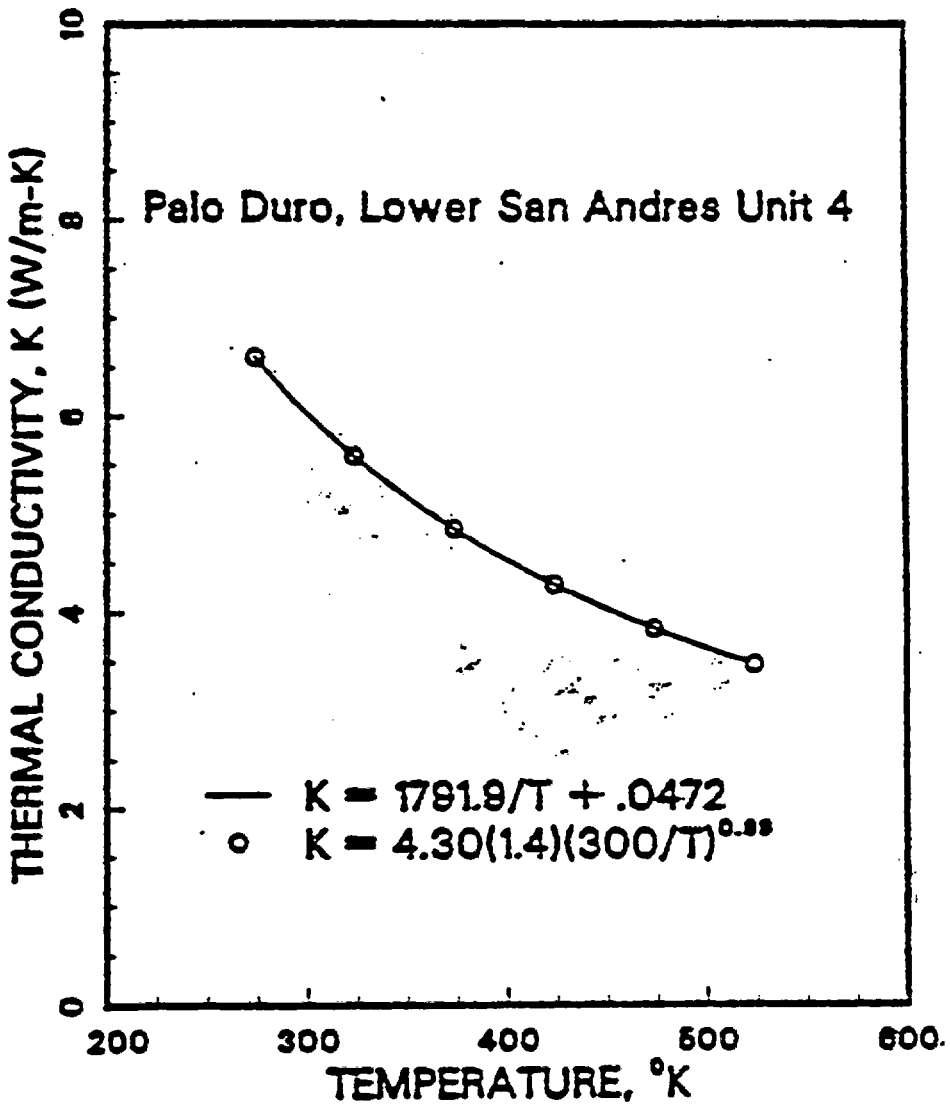

1-8

Comparison of K = A/T + B form for Thermal Conductivity with K = 1.4C (300/T)^D Relationship for Palo Duro Halite from Unit 4 of the Lower San Andres Formation

PA2 H
DC-34

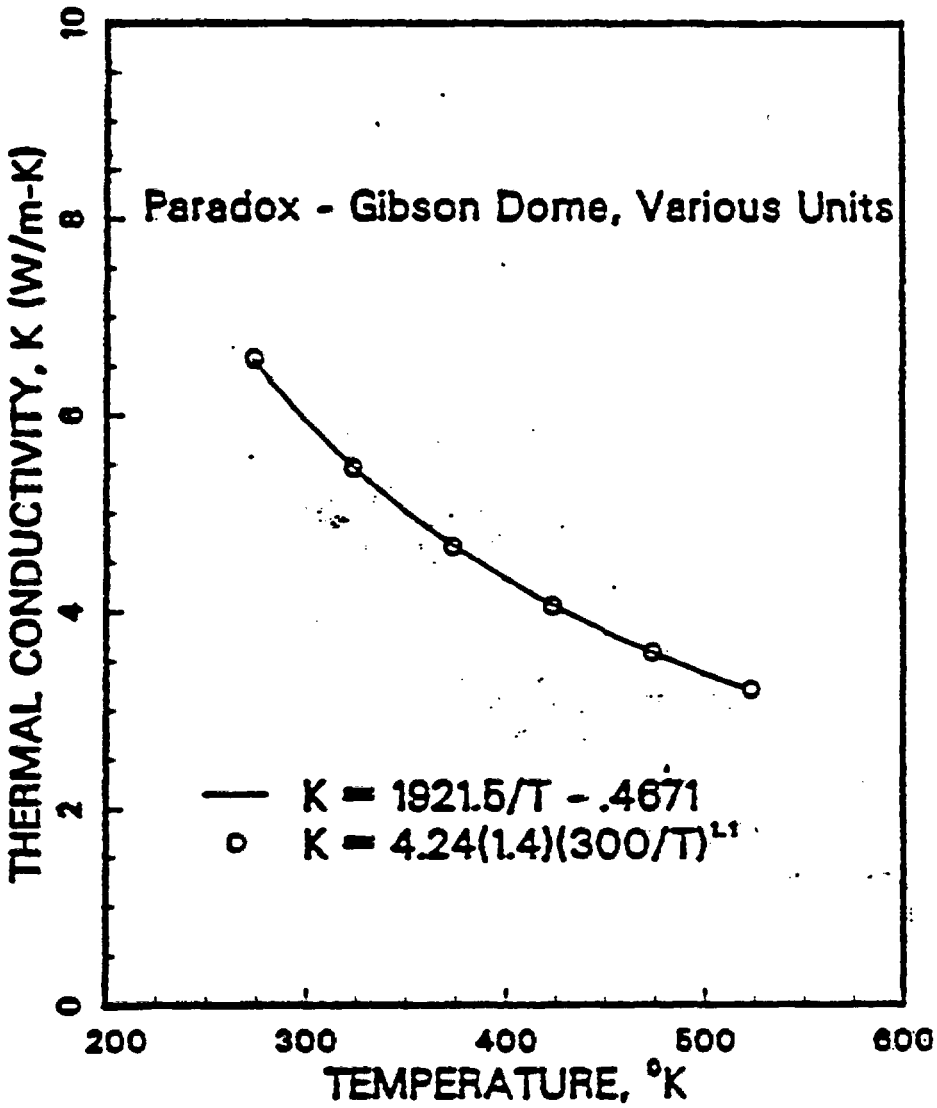

1-9

Comparison of K = A/T + B form for Thermal Conductivity with K = 1.4C (300/T)° Relationship for Various Gibson Dome Halite Units of the Paradox Formation

Fig 1-

PA2-4
DC-35

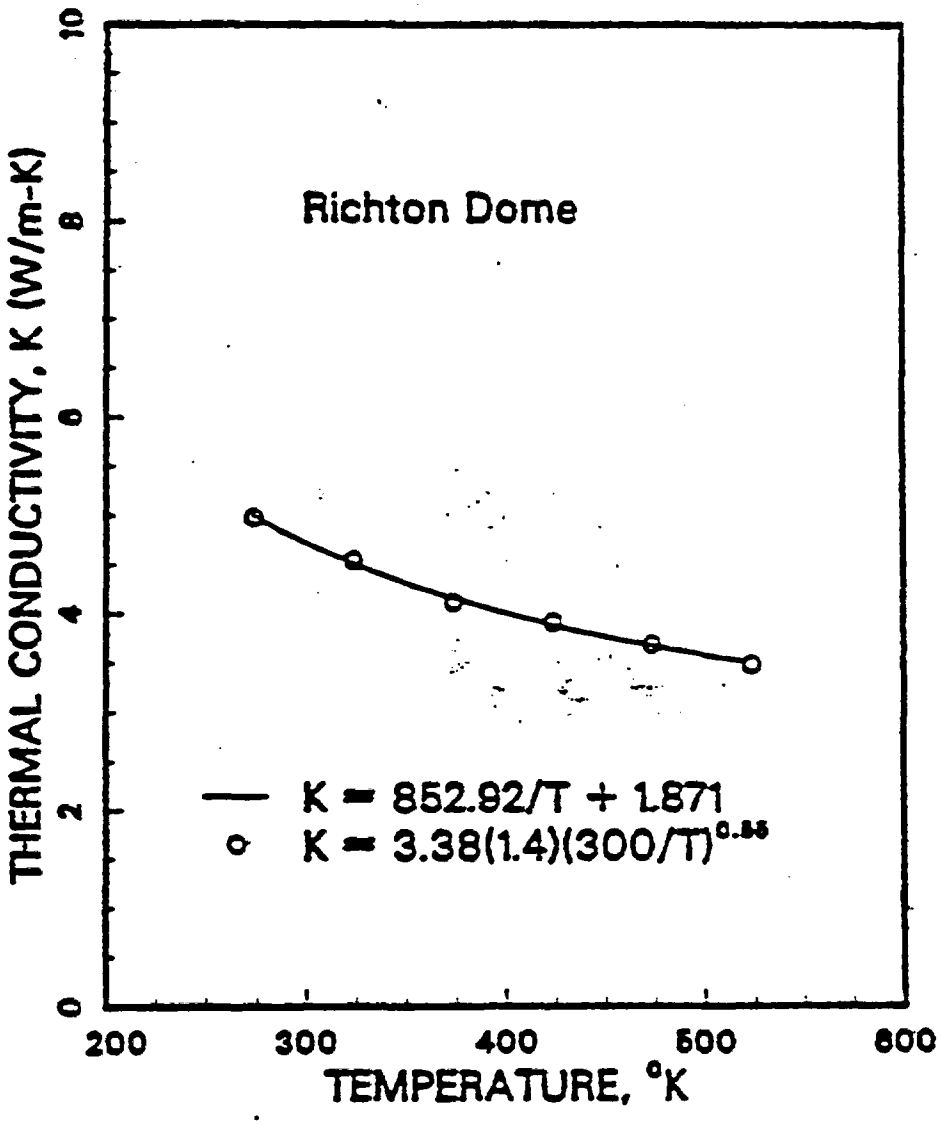

1-10

Comparison of K = A/T + B form for Thermal Conductivity with K = 1.4C (300/T)^D Relationship for Richton Dome Halite

Fig 10

FA 2H
DC 36

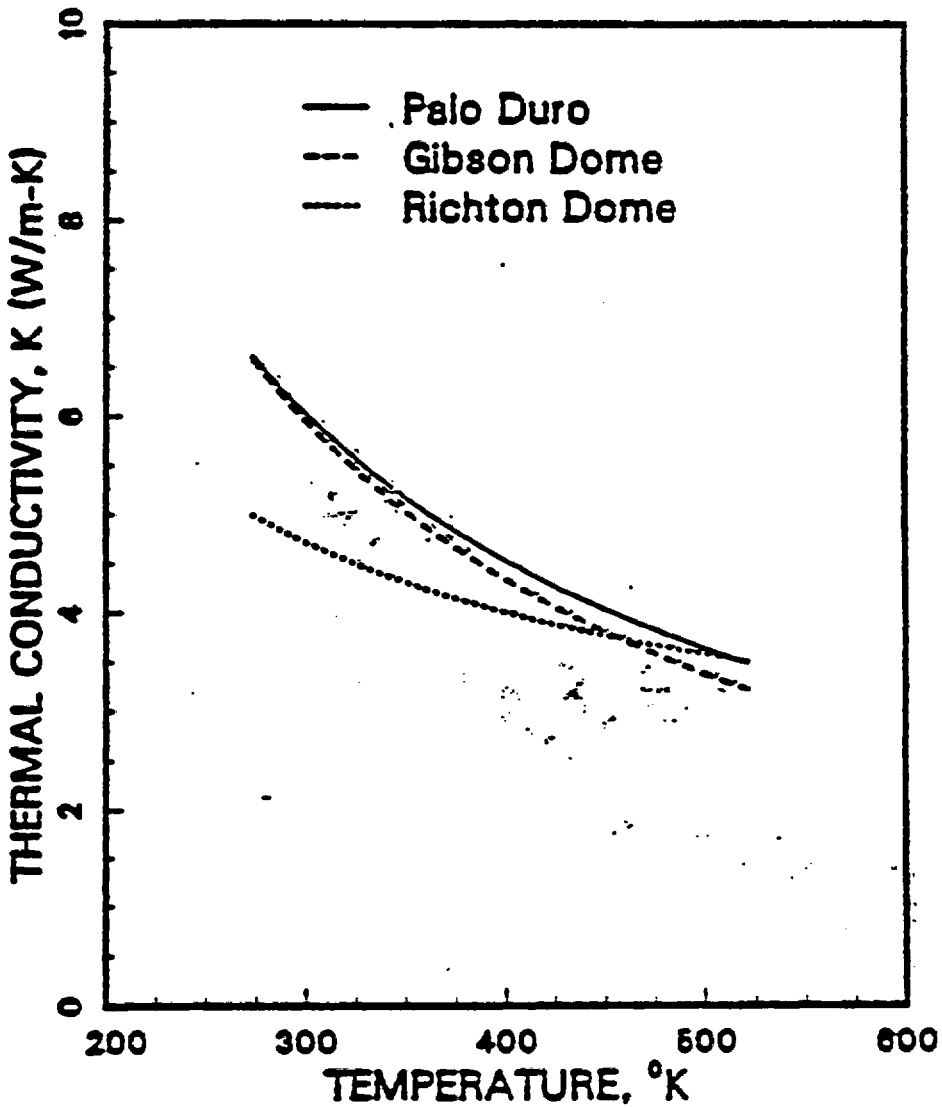

1-11

Comparison of Thermal Conductivities
of Three Salt Sites

Fig 11

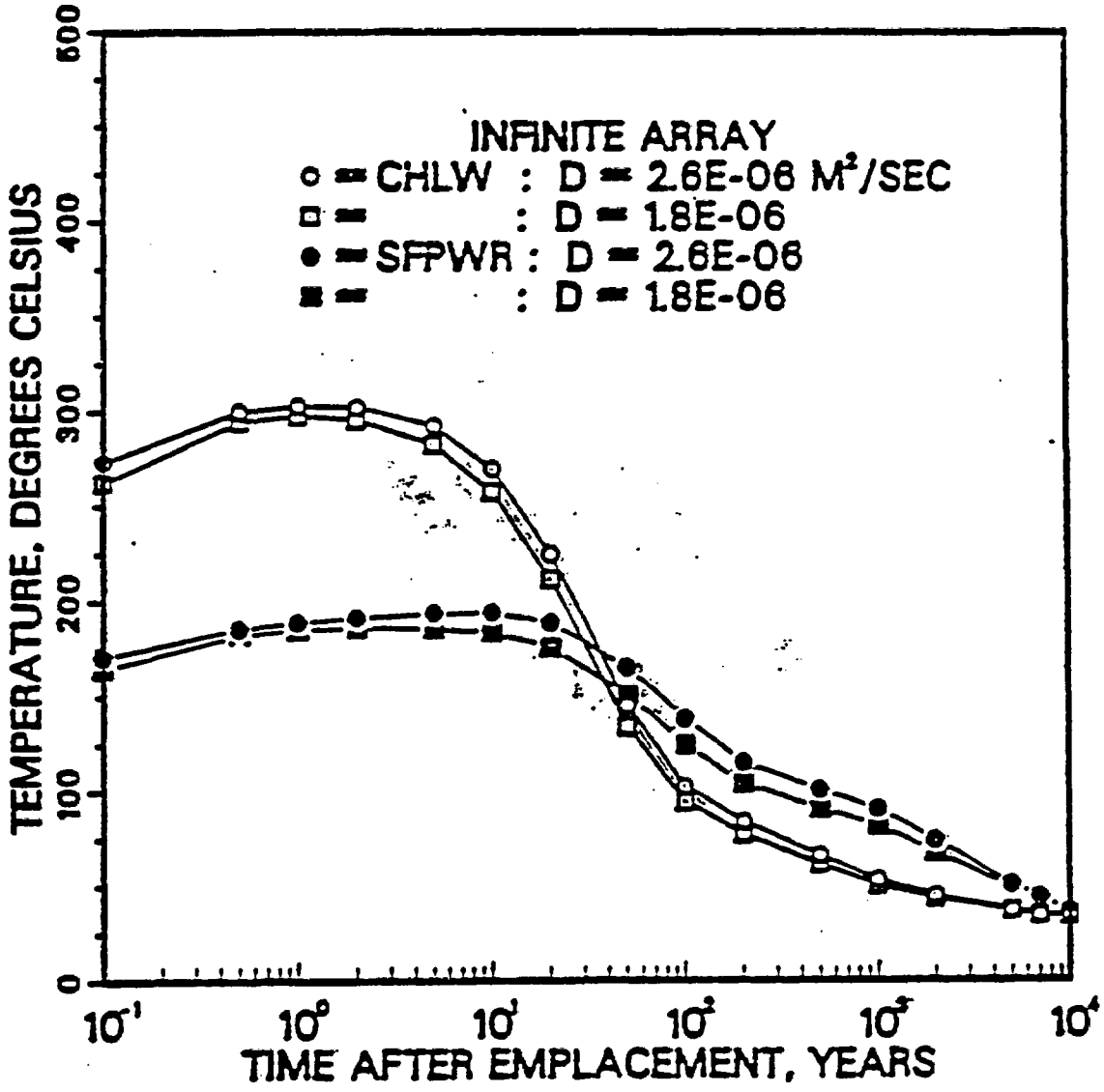

1-12

Influence of Diffusivity, D, on TEMPV5
Temperatures at Surface of Waste Package
DATA SET DIFF.FOR, 12/15 /83, SD.EAGRAPH

Fig 12

PA 2.4
DC-75

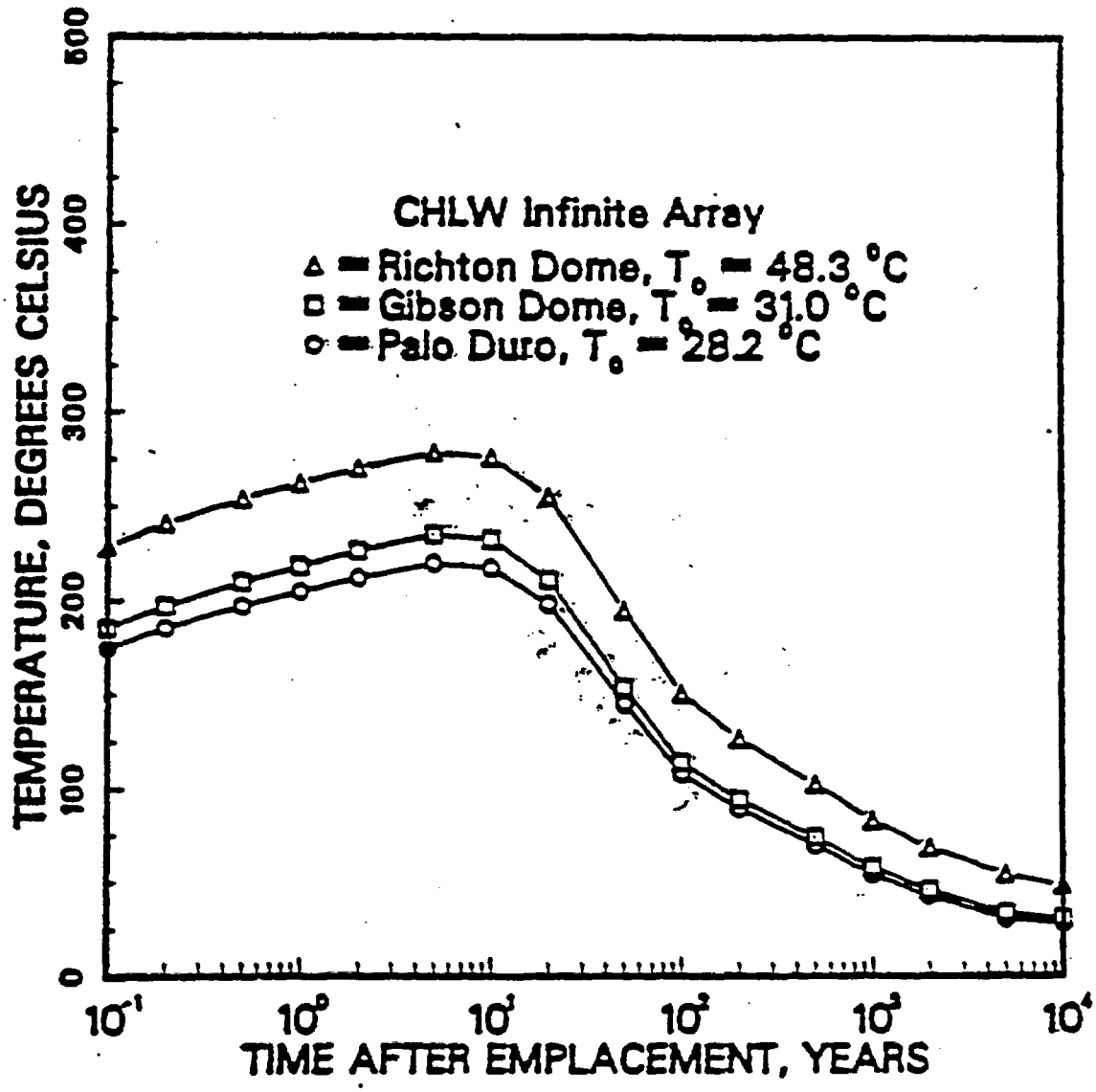

1-13

Comparison of TEMPV5 Temperatures versus Time for CHLW at Salt-Overpack Interface for Three Salt Sites

F3.13

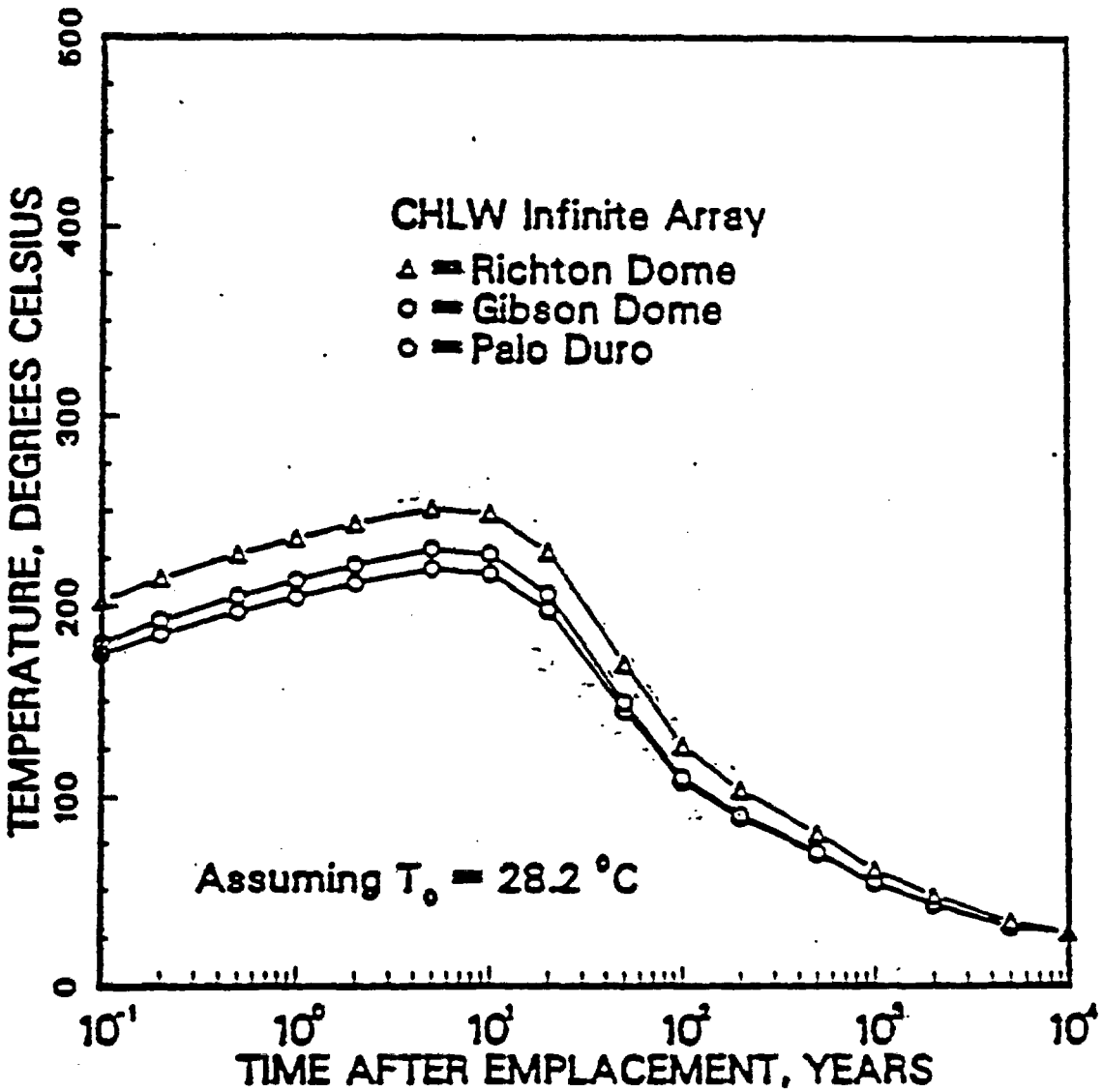

1-14

Comparison of TEMPV5 Temperatures versus Time for CHLW at Salt-Overpack Interface given Equal In Situ T_o for Three Salt Sites

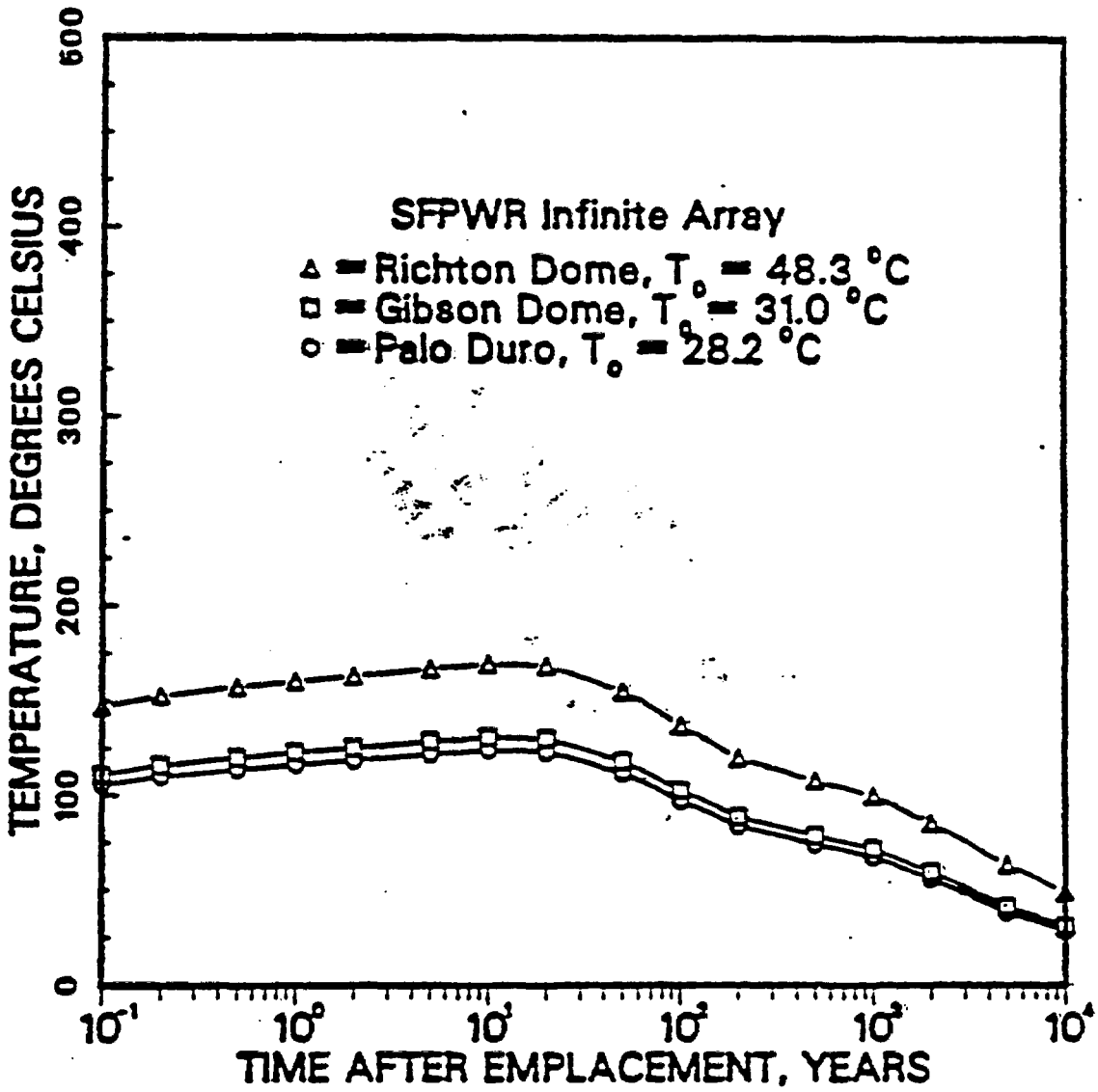

1-15

Comparison of TEMPV5 Temperatures versus Time for SFPWR at Salt-Overpack Interface for Three Salt Sites DATA SFPWR1.FOR, 01/04

Fig 15

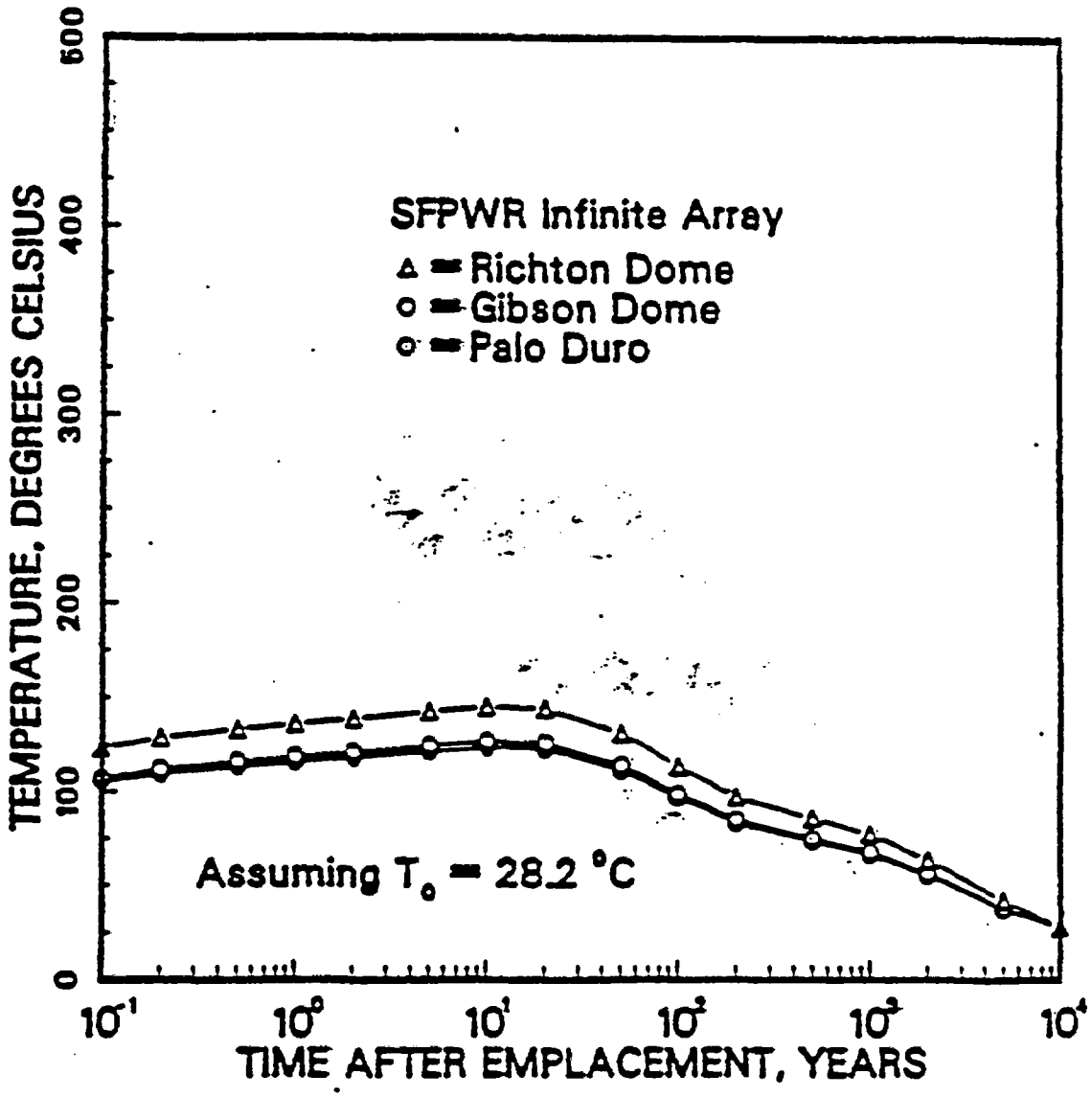

1-16

Comparison of TEMPV5 Temperatures versus Time for SFPWR at Salt-Overpack Interface given Equal In Situ T_o for Three Salt Sites
DATA SFTO.FOR 01/04/84

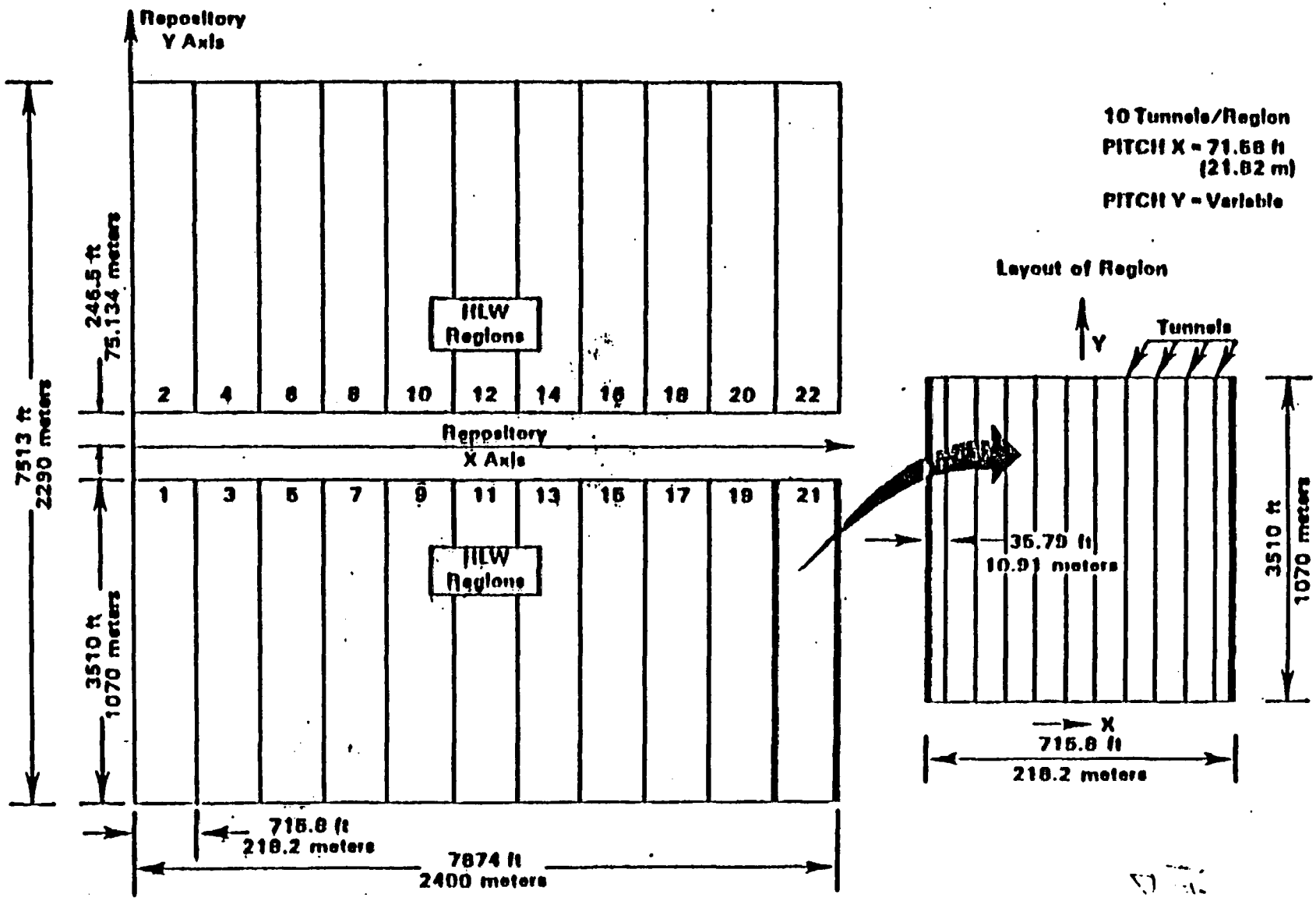

1-17 HIGH LEVEL WASTE REPOSITORY LAYOUT FOR TEMPV6 CODE

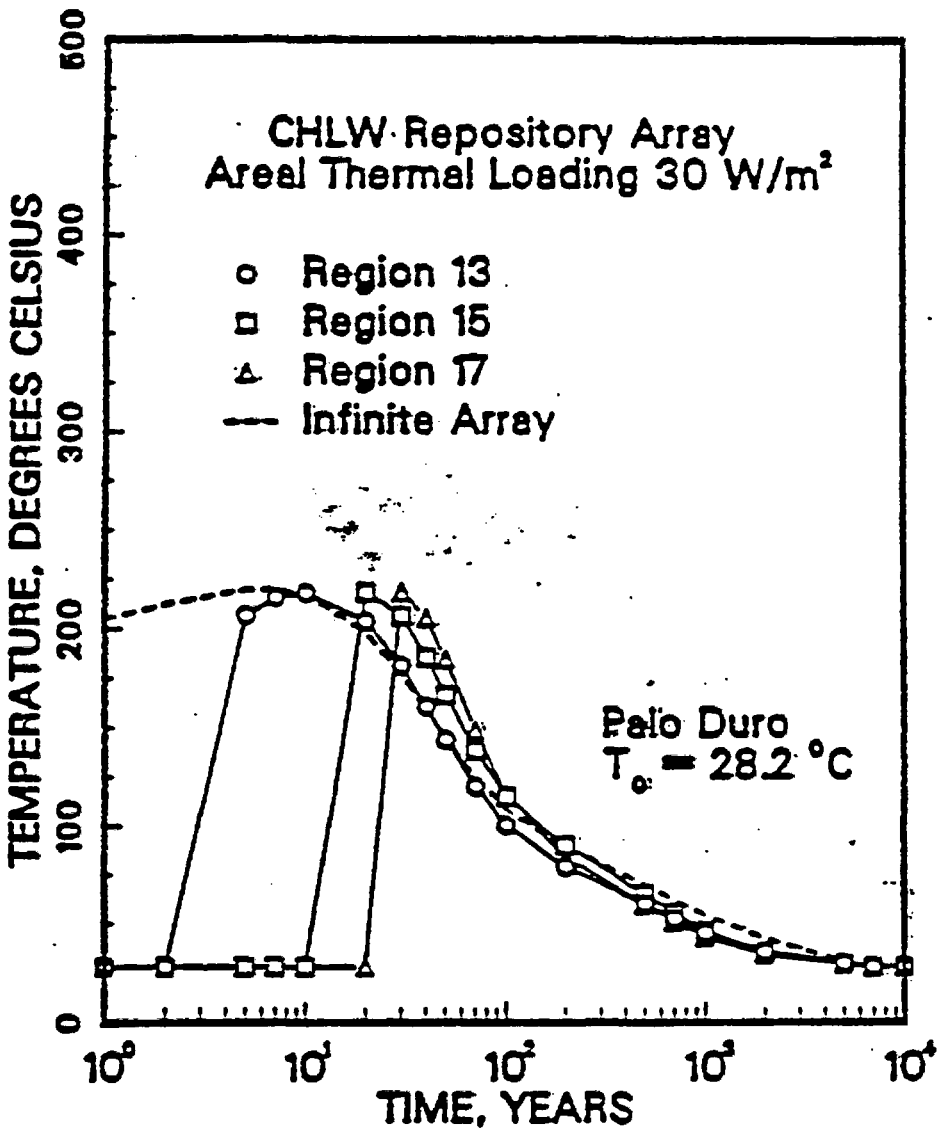

Figure 1-18

Comparison of CHLW Temperatures (TEMPV5) at Salt-Overpack Interface for Sequential Emplacement and Infinite Array Solutions.

Fig. 18

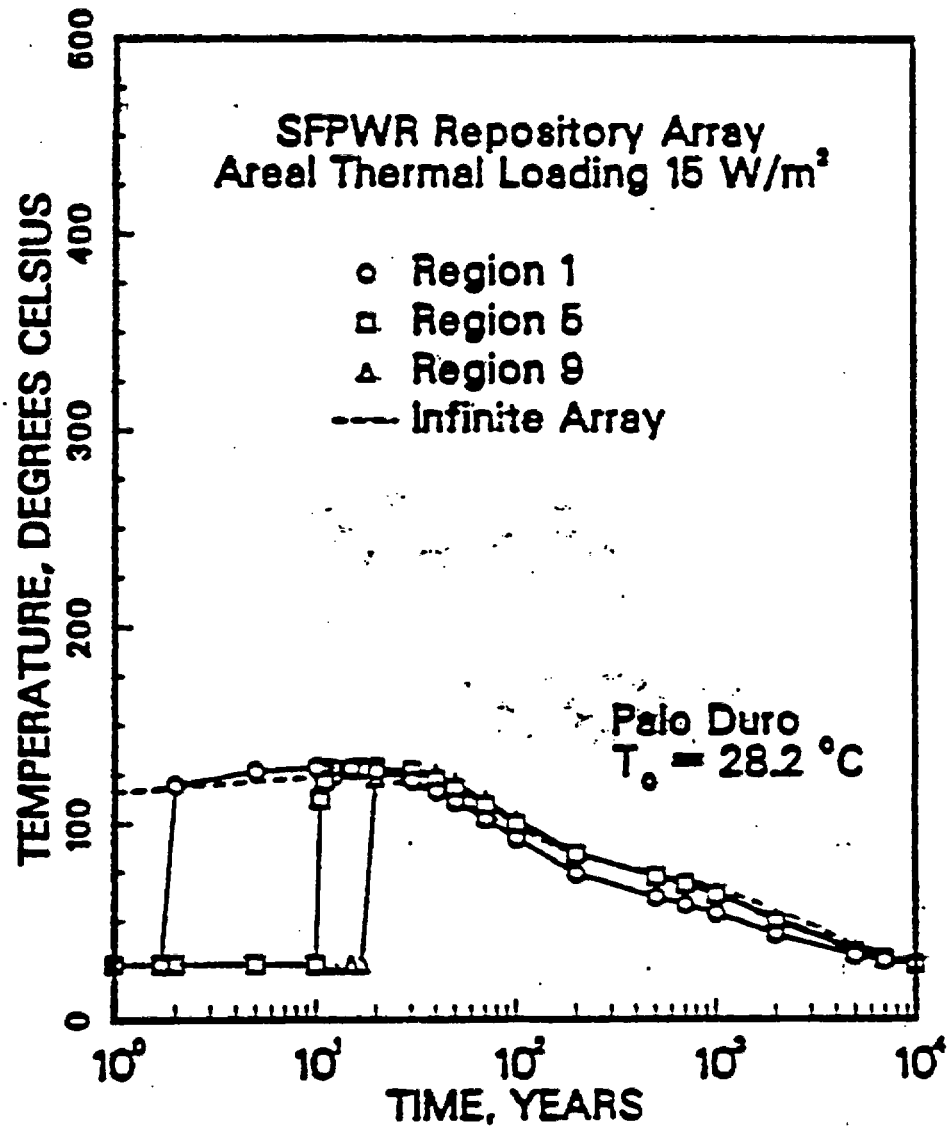

Figure 1-19

Comparison of SFPWR Temperatures (TEMPV5) at Salt-Overpack Interface for Sequential Emplacement and Infinite Array Solutions.

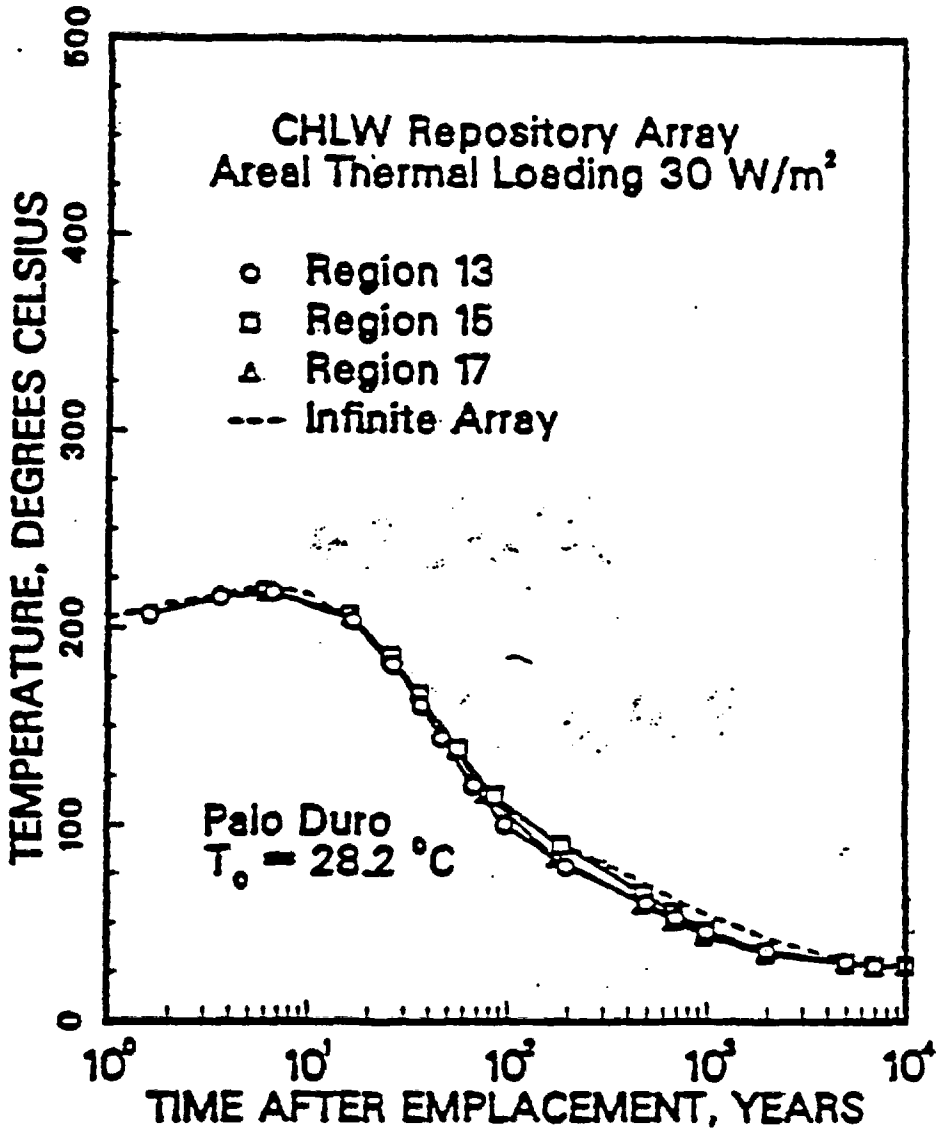

Fig 1-20

Comparison of CHLW Temperatures (TEMPV5) at Salt-Overpack Interface for Sequential Emplacement and Infinite Array Solutions.

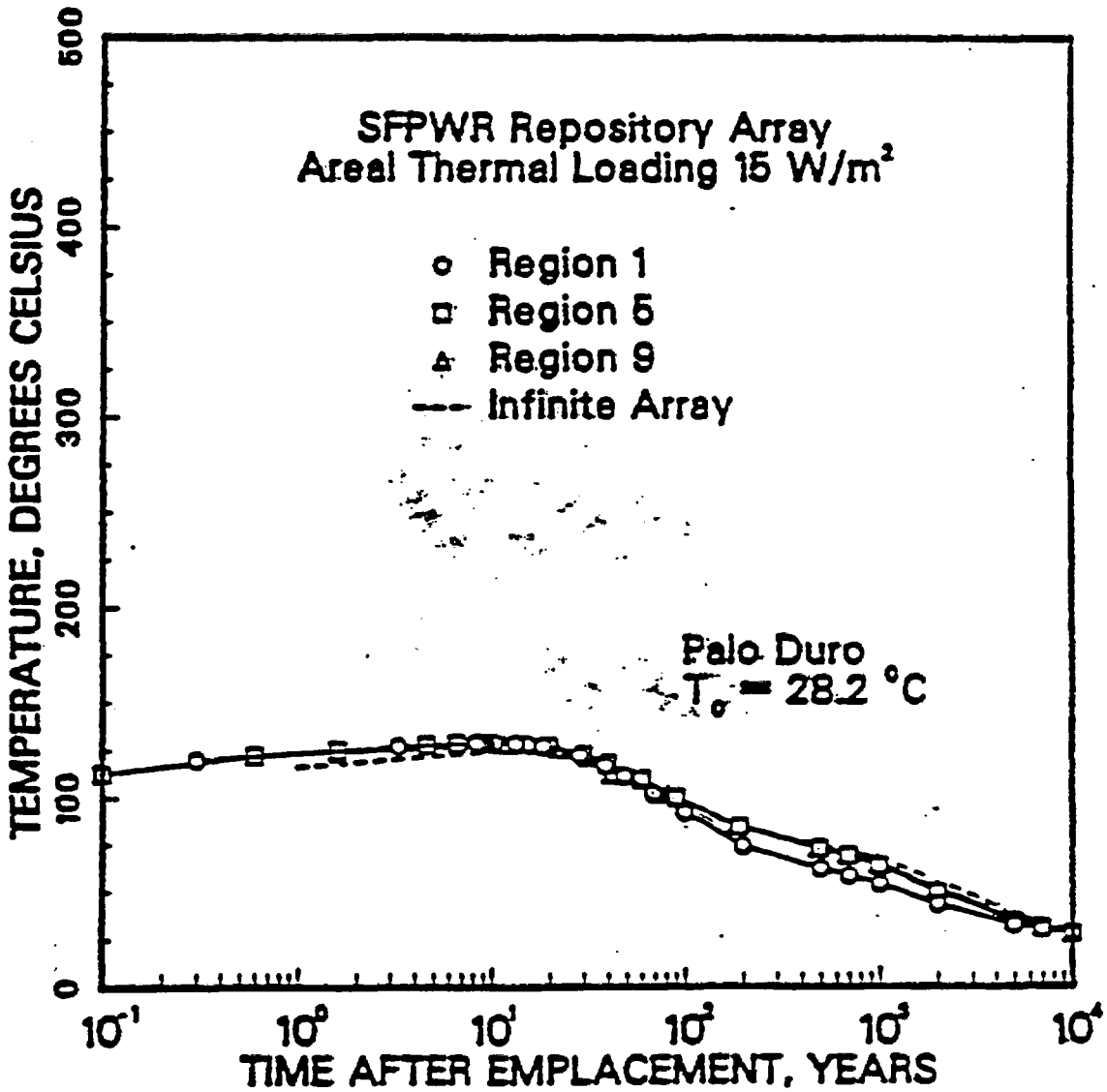

1-21

Comparison of SFPWR Temperatures (TEMPV5) at Salt-Overpack Interface for Sequential Emplacement and Infinite Array Solutions.

PART 1 of 2 Utah

Expected Nuclear Waste Repository Near-Field Performance in Three Salt Basins

Part II: Brine Migration

V. S. McCauley
G. E. Raines

PA-H
Dc. 50

2 BRINE MIGRATION

In naturally occurring salt, brine is often found trapped in small inclusions within the salt crystals and along crystal boundaries. When a thermal gradient is applied, two types of brine migration therefore occur. The first is intracrystalline brine migration, which consists of the migration of individual brine inclusions. The second is intercrystalline migration, which deals with the movement of brine through the intercrystalline network.

Intracrystalline migration is well understood. When a thermal gradient is applied to a brine inclusion, the solubility of salt in the brine increases at the hot face of the inclusion. The result is dissolution of salt at this face. The dissolved salt is transported across the inclusion to the cooler face, causing the brine there to become supersaturated. Precipitation of salt at the cooler face of the inclusion results. Through this continuing process of dissolution, transport, and precipitation, the brine inclusion slowly migrates through the salt crystal. Dissolution of salt at the hot face is the rate-limiting step.

Each inclusion migrates in this manner until it reaches a crystal interface. At this point intracrystalline migration is observed to stop--the inclusion is unable to migrate through the crystal boundary. Instead the brine in the inclusion passes into the intercrystalline network and continues to migrate toward the heat source. Intercrystalline movement is not as well understood, but is probably the result of pressure gradients. It has generally been modeled assuming Darcy flow.

Elaborate theories of brine migration have been developed, as have codes which use these theories to model brine migration. However use of the codes as predictive tools is impossible because the data required by these codes are not available. To overcome this problem in the present study, a simple finite difference code was developed to predict brine migration quantities and migration rates over a 10,000 year period. A minimum amount of information is required to make predictions of brine migration using this code.

2.1 BACKGROUND

Olander, Machiels and Yagnik (1980) developed a detailed theory of intracrystalline brine migration in KCl and NaCl which described the migration

PA2 H
DC 50

of all-liquid inclusions and gas-liquid inclusions. For all-liquid inclusions they reported that velocities varied widely, but were roughly a function of the square of the temperature gradient. Intercrystalline migration was not examined.

Although gas-liquid inclusions have been observed in salt samples, it is not known whether they occur at repository depth. They may only be an artifact of the removal and transport of the salt samples. It is also not known whether they might be formed by radiolysis at the repository site. They are of interest because they migrate away from the heat source, by a continuing process of evaporation of moisture and precipitation of salt at the hot face, diffusion of water vapor through the gas phase, dissolution of salt by condensing moisture at the cool face, and transport of salt through the liquid. Since the fraction of brine contained in gas-liquid inclusions is not known, a conservatively high estimate of the amount of brine expected to reach a waste package may be made by assuming that all inclusion brine is contained in all-liquid pockets.

Jenks and Claiborne (1981) analyzed the literature on brine migration and developed the Jenks equation,

$$\log(V/G) = 0.00656\ T - 0.6036 \qquad (2\text{-}1)$$

where V = velocity of brine migration, cm/y
G = temperature gradient, degrees C/cm
T = temperature, degrees C,

to calculate the velocity of brine migration in salt. The Jenks equation was developed to give conservatively high velocities based on available data on intracrystalline brine migration. No attempt was made to model intercrystalline migration separately. The authors instead applied the Jenks equation to the overall brine migration problem, including both intracrystalline and intercrystalline flow, and attempted to validate their code with Salt Block II data (Hohlfelder, 1980). The resulting program, called MIGRAIN, modeled the data reasonably well.

is this conservative?

The available data on brine migration velocities show a very wide scatter. The velocity of a single migrating inclusion can vary by a factor of four as the inclusion moves through a salt crystal (Olander, 1980, p. 4). The explanation offered by Olander, Machiels and Yagnik is that dislocations which intersect the dissolving salt front increase the rate of dissolution at the hot

PA 2-4
DC 51

face. Because dissolution is the rate-limiting step, an increase in the rate of migration of the inclusion results.

Because of the wide scatter in velocity data which occurs, it is not possible to determine whether the relationship described by Olander, et al or the Jenks equation gives a better fit to the data. The Jenks equation was developed to give maximum velocities, though, which makes it useful for conservative calculations. Further, the Jenks equation was used with some success in the MIGRAIN code.

A parameter critical to brine migration calculations is the initial moisture content of the salt. A review by Roedder and Chou (1982, pp. 2-8) listed a maximum observed moisture content of 1.7 weight percent for bedded salts. For domal salts, a value of 0.1 weight percent was suggested for conservative calculations. The conservatism of the maximum value for bedded salt is not well understood because of impurities in the salt beds, such as hydrated minerals, which are expected to contribute moisture at high temperatures. However an assumed average moisture content of 1.7 weight percent should be conservative except in regions of anomalously high moisture content. Such regions would not be considered suitable repository sites. The moisture content the authors suggested for domal salt should be very conservative. The impurities which are prevalent in salt beds are not as important a problem in domal salt.

One other source of moisture may have to be considered. The crushed salt used to backfill the repository could contain excess moisture picked up during storage. It may be necessary to limit the mosture content of this backfill to prevent too much brine from reaching the waste packages. Certainly this possibility needs to be examined.

Theoretical considerations indicate the existence of a threshold temperature gradient below which brine cannot migrate (Jenks, 1981, p.96). Jenks and Claiborne (1981, pp. 96-103) calculated a series of values for the threshold gradient; a value of 0.125 degrees C/cm was used by them for temperatures below 100°C. The concept of a threshold gradient in sodium chloride crystals is not universally accepted, however (Roedder, 1982, pp.20-21). Therefore a conservative estimate of brine migration must include the zero threshold gradient case.

FA 2 H
DC 52

2.2 THE BRINE MIGRATION COMPUTER PROGRAM

An explicit time marching finite difference code was developed to predict rates of brine migration to a nuclear waste package. Called BRINEMIG, it uses mass balances over a series of radial increments to develop concentration profiles at regular time steps and to calculate brine flow to the package surface with time. The Jenks equation is used in the mass balance calculations to calculate brine migration velocities. The brine migration phenomenon is treated as a one-dimensional problem.

As stated in the Introduction, the Jenks equation is an empirical equation based on intracrystalline flow. No such simple equation to predict intercrystalline flow is presently available. Therefore, to keep the model simple, intercrystalline and intracrystalline velocities were assumed to be equal. At present, the only justification for making this assumption was the success of the MIGRAIN code in predicting brine migration rates. MIGRAIN made the same simplifying assumption. Good?

The BRINEMIG code requires two pieces of information about the site being modeled. The first is an initial moisture content of the salt. As the program is presently written, a single value must be used to represent the site. The program does not accommodate local variations in brine quantity. The second piece of information needed is a one-dimensional temperature profile representing the site. This is read by BRINEMIG in a tabular form with temperatures given as functions of both radius and time. Semilogarithmic interpolations are performed to estimate temperatures within the range of the table; extrapolations are not performed. Temperature gradients are approximated conservatively by calculating the change in temperature over a radial increment rather than by approximating the gradient directly. The only exception is at the waste package surface where no previous radial increment exists.

Because predictions of velocity by the Jenks equation rely so heavily on the temperature gradient, the method used for approximating this gradient directly affects the results. Approximating over the radial increment overestimates the temperature gradient; the estimate approaches the exact solution as smaller radial increments are taken. It is therefore useful to run BRINEMIG at several radial increments to reduce this overprediction and to

FA 4
DC 53

have an idea how much conservatism this approximation is contributing to the final solution.

At each time increment the program steps over a series of radial increments from the package surface to a specified stopping point in the salt. For the mth radial increment and the nth time increment, a simple mass balance yields

IN = OUT + ACCUMULATION

$$V_m A_m c_{n,m+1} = V_{m-1} A_{m-1} c_{n,m} + (c_{n+1,m} - c_{n,m}) \frac{\Delta v_m}{\Delta t} \qquad (2\text{-}2)$$

where each subscripted V represents a velocity calculated by the Jenks equation; each subscripted c represents a concentration of moisture in the salt; Δv_m is the volume between the (m-1)th and mth nodes over a unit length, equal to

$$\Delta v_m = 2\ \pi m (\Delta r)^2 \left(1 - \frac{1}{2m}\right) \qquad (2\text{-}3)$$

where Δr is the radial increment and m represents the radial increment number; Δt is the time increment; and each subscripted A represents the surface area over a unit length at the radial node indicated by the subscript. The areas may be expressed as

$$A_m = 2\pi m \Delta r \qquad (2\text{-}4)$$

$$A_{m-1} = 2\pi (m-1) \Delta r. \qquad (2\text{-}5)$$

Substituting Equations 2-3, 4, and 5 into Equation 2-2 and solving for c gives the final brine migration equation,

$$c_{n+1,m} = c_{n,m}\left[1 - V_{m-1,n} \frac{(1-\frac{1}{m})\ \Delta t}{\Delta r(1-\frac{1}{2m})}\right] + c_{n,m+1}\left[\frac{V_{m,n}\Delta t}{\Delta r(1-\frac{1}{2m})}\right] \qquad (2\text{-}6)$$

PA2 4
3C50

Equation 2-6 is stable only when

$$V_{m-1,n} \frac{(1-\frac{1}{m})\Delta t}{\Delta r(1-\frac{1}{2m})} < 1 \qquad (2\text{-}7)$$

If the stability criterion is exceeded, the program will stop executing. The parameters Δt and Δr must be adjusted until stability is assured.

Flow into the borehole equals the flow out of the first radial increment. Therefore the quantity, Q_n, of accumulated brine over the nth time increment is given by

$$Q_n = V_o A_o \Delta t \; (c_{n,1} + c_{n+1,1})/2 \qquad (2\text{-}8)$$

where subscript o indicates the package surface. The area may be expressed as

$$A_o = 2\pi \; rL \qquad (2\text{-}9)$$

where L is the effective package length and r is the package radius. Substituting Equation 2-9 into Equation 2-8 gives

$$Q_n = \pi \; rLV_o \Delta t(c_{n,1} + c_{n+1,1}) \qquad (2\text{-}10)$$

Summing Q_n over each time step gives the total brine accumulation with time. The effective package length, L, is an important parameter. Because only radial flow is modeled by BRINEMIG, a package length must be chosen which will reflect the added flow at the package ends. This will be discussed further in later sections.

2.3 PRELIMINARY VALIDATION

A preliminary validation was made with Salt Block II brine migration data (Hohlfelder, 1980); the details are presented here. A long term brine migration study is presently under way in the Asse Mine, Federal Republic of Germany (Westinghouse, 1983a). As the Asse data are made available, they will be used to attempt a further validation of the BRINEMIG code.

PA 2 +
Dc 55

The Salt Block II experiment (Hohlfelder, 1980) was a brine migration study performed on a cylindrical salt sample from bedded salt in southeastern New Mexico. The cylinder was 1 meter high and 1 meter in diameter, and had a borehole along its axis that was 0.8 meters long and 0.13 meters in diameter. An electrical heater was placed in the borehole along with crushed salt backfill, and a cooling jacket was placed along the outside wall of the cylinder. The ends of the cylinder were insulated.

When the heater and cooling jacket were turned on, brine began to migrate toward the heat source. As the brine entered the borehole, dry nitrogen gas was swept through the borehole to carry the moisture away. The rate at which moisture entered the borehole was determined by analyzing the exiting gas stream for moisture content. By this means a data set of brine migration versus time was developed.

The heater output was changed periodically so that the effect of temperature on brine migration could be determined. First the heater output was raised, then lowered in discrete steps. The resulting sudden temperature changes apparently stressed the salt, because relatively rapid, short-term flow rates resulted. The increased flow was particularly noticeable for the temperature reductions.

Temperature profiles for the Salt Block II study were calculated by a two-dimensional thermal model and validated with thermal data taken during the course of the experiment (George, 1980). The results of the model were published in a more detailed form by Hohlfelder (Hohlfelder, 1980). To validate BRINEMIG, the most conservative one-dimensional radial profiles calculated by George's thermal model (those with the highest temperatures and largest thermal gradients at each heater output level) were selected to represent the Salt Block II system. Table 2-1 lists these temperatures and corresponding times.

Figure 2-1 compares the results of semilogarithmic interpolation to the results of George's thermal model for the worst-case temperature profile predicted at the highest heater output. A semilogarithmic interpolation was performed by BRINEMIG between the inside and outside radii listed in Table 2-1. The agreement between the two models is reasonable, justifying the use of semilogarithmic interpolation for temperature calculations.

For this preliminary validation, the decision was made to model only the first phase of the Salt Block II experiment, in which temperatures were raised

in discrete steps. Since sudden temperature drops are not expected in a repository, the large transient flows associated with temperature drops are not realistic for a repository. For input to BRINEMIG, the heater length of 0.6 meters was selected as the effective package length. This effective length was not
conservative because end effects were neglected. In addition, an initial moisture content in the salt of 0.5 volume percent was assumed. This falls within the range of measured moisture contents in the salt (Hohlfelder, 1980, p.32).

Results of the simulation are shown in Figure 2-2. At the higher temperatures, BRINEMIG overpredicts the brine migration rate. At lower temperatures, agreement with data is closer. Overall, the results support use of the Jenks equation to predict velocities of migration, even though it was not developed based on intercrystalline flow. However further refinements to the calculational procedure are needed. In particular, a way to model flow to the waste package at the ends of the cylinder needs to be incorporated into the code, to assure conservatism in this area. The effect of the temperature profile on the brine migration rate should also be studied, to give an idea of the expected variation in migration rate along the length of the waste package.

Figure 2-3 shows the final concentration profile predicted in the salt. A depletion is predicted in the region near the borehole. Hohlfelder's report presents some evidence that this occurs, but the method used to test the samples makes the results uncertain. Intuitively, a depletion near the borehole seems likely.

2.4 MODELING OF BRINE MIGRATION IN SALT REPOSITORIES

Three proposed repository sites in salt were modeled, along with two waste forms. The sites considered were Gibson Dome and Palo Duro bedded salts and Richton Dome; the waste forms studied were commercial high-level waste (CHLW) and spent fuel (SFPWR). In addition, studies were made with and without a threshold gradient. All twelve combinations of cases were run using BRINEMIG.

To be consistent with the Salt Block II preliminary validation, effective package lengths were assumed to be equal to the heat-producing lengths of the packages. For CHLW this was 367.9 cm and for SFPWR it was 385.0 cm. The

PA2 DC-57

borehole radius was assumed equal to the package radius in each case. For CHLW this was 44.5 cm and for SFPWR it was about 41.76 cm (Westinghouse, 1983b, Tables 1-2 and 1-3, Alt. II).

Site specific moisture content data are not available for the sites. Considerable work would need to be done to establish a moisture content for a repository site due to the large local variations in this property. To assure conservatism, large moisture contents were assumed, even by the standards of Roedder and Chou (see Background). For the bedded salt sites, an initial moisture content of 5 volume percent was selected; for the domal site, 0.5 volume percent was chosen.

Because of the Jenks equation, temperature profiles showing the highest temperatures and the steepest thermal gradients will show the highest brine migration rates. In a nuclear waste repository, the highest temperatures are expected at the midpoint of the package length; the steepest gradients are expected where the distance between packages is greatest. The most conservative temperature profiles should therefore occur at the package midpoint, in the direction between rooms of the repository. These are the profiles which were used for modeling brine migration with BRINEMIG. They were supplied in tabular form by the program TEMPV5. (See Section 1, Thermal Conditions.)

For two identical waste forms, assuming a uniform salt bed, a symmetrical temperature profile is expected between waste packages. A zero thermal gradient is therefore expected at the midpoint between packages. Since the Jenks equation predicts zero migration at a zero threshold gradient, calculations of brine migration need only be made from the package surface to midway between packages to account for all migration to a package. In practice, the migration rate becomes negligible well before the midpoint is reached.

Figures 2-4, 2-5 and 2-6 present selected temperature profiles for CHLW at the three salt sites. Figures 2-7, 2-8 and 2-9 present temperature profiles for SFPWR. In each case, the radius is measured from the center line of the package. Initially, CHLW shows higher temperatures and steeper thermal gradients near the waste package. Temperatures remain elevated longer for SFPWR. For both waste forms, Richton Dome shows the highest temperatures overall, and Palo Duro shows the lowest.

Figures 2-10 through 2-15 present results of BRINEMIG, first for the zero threshold gradient case, then for a threshold gradient of 0.125 degrees C/cm.

P#24
DC 58

The total accumulated flows predicted are listed in Table 2-2. As expected, the use of a threshold gradient below which flow is assumed to cease results in lower quantities of accumulated brine, with the largest differences occurring in the case of SFPWR. In every case, the amounts of accumulated brine for CHLW are higher than those for SFPWR.

Richton Dome shows the lowest quantities of accumulated brine in every case. The large difference in assumed moisture content between the beds and the dome far outweigh the higher temperatures at Richton for determining the amount of brine migration. These lower numbers make Richton look the most favorable as a repository site from the perspective of brine migration. However if so little brine migrates that the waste forms never fail, the relative amounts of accumulated brine become unimportant. This must be determined by waste package analysis.

Figure 2-16 shows the concentration profile predicted by BRINEMIG for CHLW at Gibson Dome after 10,000 years. It appears that some sort of harmonic effect has been introduced by the finite difference method, since the irregularity increases with the number of iterations. However the rates of accumulation at large times look reasonable, even though the concentration profiles do not.

2.5 CONCLUSIONS AND RECOMMENDATIONS FOR FURTHER WORK

The most important improvement which ought to be made to the BRINEMIG code is to account for two-dimensional migration to the waste package. Such a modification would allow the effect of changes in the temperature profile along the package length to be accounted for, and flow from beyond the ends of the effective package length to be calculated.

More site-specific information is needed about the sources of moisture available for migration. The importance of moisture in the crushed salt backfill, possible release of moisture from hydrated minerals, effects of clay interbeds and other impurities, and possible effects of radiolysis should be examined. Also, the reasonableness of using the Jenks equation to model intercrystalline migration needs to be examined further. An attempt at validation using Asse Mine data should support or refute use of this equation.

If package failure is ever expected, Richton Dome looks best from the point of view of brine migration. Because of the much lower expected moisture

content in a salt dome, not as much brine is available at Richton to migrate to the waste packages. Improvements to the BRINEMIG code are not likely to change this result. However if package failure is not expected even at Gibson Dome, the relative amounts of migration to the waste packages become fairly unimportant.

REFERENCES

George, Oscar L. Jr., 1980. Computer Thermal Modeling for the Salt Block II Experiment, SAND79-2250, Sandia National Laboratories, Albuquerque, NM.

Hohlfelder, Jacque J., 1980. Salt Block II: Description and Results, SAND79-2226, Sandia National Laboratories, Albuquerque, NM.

Jenks, G. H. and H. C. Claiborne, 1981. Brine Migration in Salt and Its Implications in the Geologic Disposal of Nuclear Waste, ORNL-5818, Oak Ridge National Laboratory, Oak Ridge, TN.

Olander, D. R., A. J. Machiels, and S. Yagnik, 1980. Thermal Gradient Migration of Brine Inclusions in Salt, ONWI-208, Office of Nuclear Waste Isolation, Battelle Memorial Institute, Columbus, OH.

Roedder, Edwin and I-Ming Chou, 1982. A Critique of "Brine Migration and Its Implications in the Geologic Disposal of Nuclear Waste," Oak Ridge National Laboratory Report 5818, by G. H. Jenks and H. C. Claiborne, Open-File Report 82-1131, U. S. Geological Survey, Reston, VA.

Westinghouse Electric Corporation, 1983a. Brine Migration Test for Asse Mine, Federal Republic of Germany: Final Test Plan, ONWI-242, prepared for Office of Nuclear Waste Isolation, Battelle Memorial Institute, Columbus, OH.

Westinghouse Electric Corporation, 1983b. Engineered Waste Package Conceptual Design: Defense High-Level Waste (Form 1), Commercial High-Level Waste (Form 1), and Spent Fuel (Form 2) Disposal in Salt, ONWI-438, prepared for Office of Nuclear Waste Isolation, Battelle Memorial Institute, Columbus, OH.

DA 24
DC 80

Table 2-1. Temperature Profiles Used as Input to BRINEMIG for Simulation of Salt Block II Data

Time, Yr		Temperature, Degree C	
Initial	Final	At Borehole	At Outside Radius
0.0001	0.01615	18.4	18.4
0.01715	0.03530	41.5	24.1
0.03630	0.05453	62.4	29.8
0.05553	0.09555	87.7	35.4
0.09655	0.13409	137.1	45.9
0.13509	0.32264	206.2	58.4

1000 K at 1000 yr

Table 2-2. Total Quantities of Accumulated Brine

Site	Threshold Gradient, degrees C/cm	Accumulated Brine, liters CHLW	SFPWR
Gibson	0.125	900	425
Gibson	0.0	994	754
Palo Duro	0.125	788	372
Palo Duro	0.0	878	684
Richton	0.125	149	76
Richton	0.0	166	131

PA2-11
DC-62

Figure 2.1 thru 2.16 (sixteen pages)

Type 17 [illegible]

PA 2 H
DC B

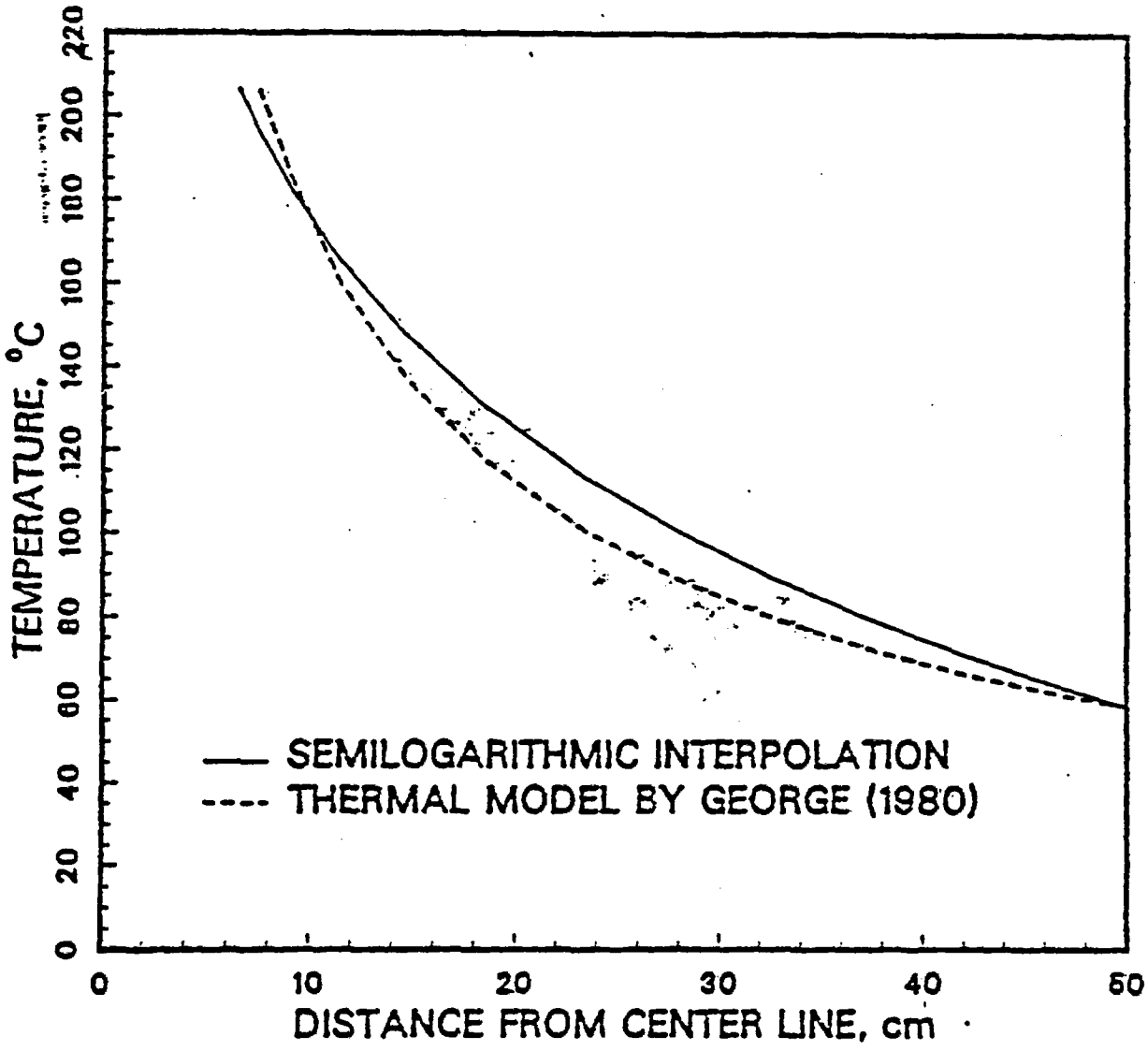

Comparison of Temperature Profiles for Salt Block II
BRINEMIG Thermal Calculation vs. Two-dimensional Code

Figure 2.1

FA2 H
DC 14

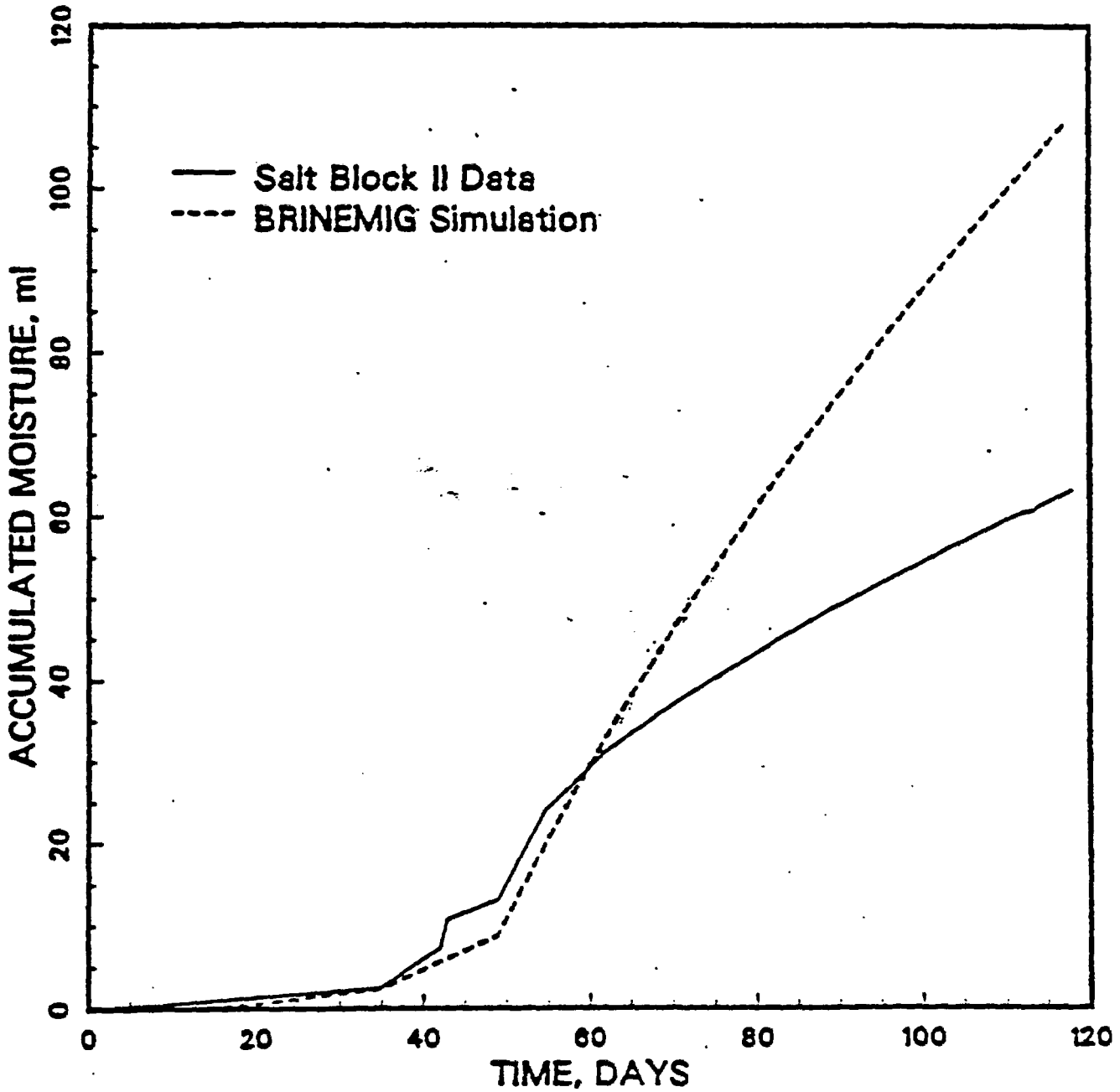

Figure 22 Accumulated Moisture vs. Time
Simulation of Salt Block II Data

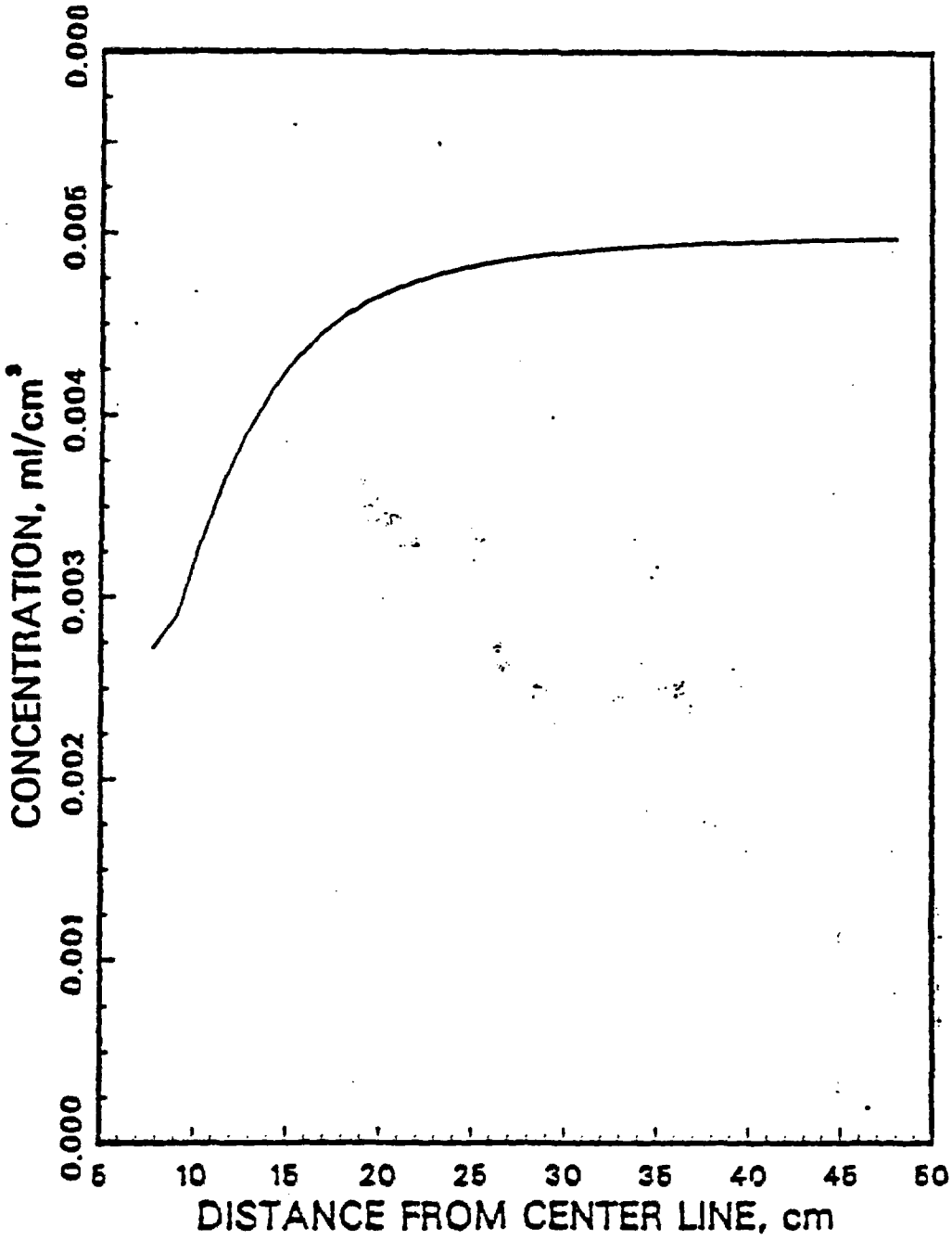

Figure 2.3 Final Concentration Profile for Salt Block II Simulation

AA2-H
DC66

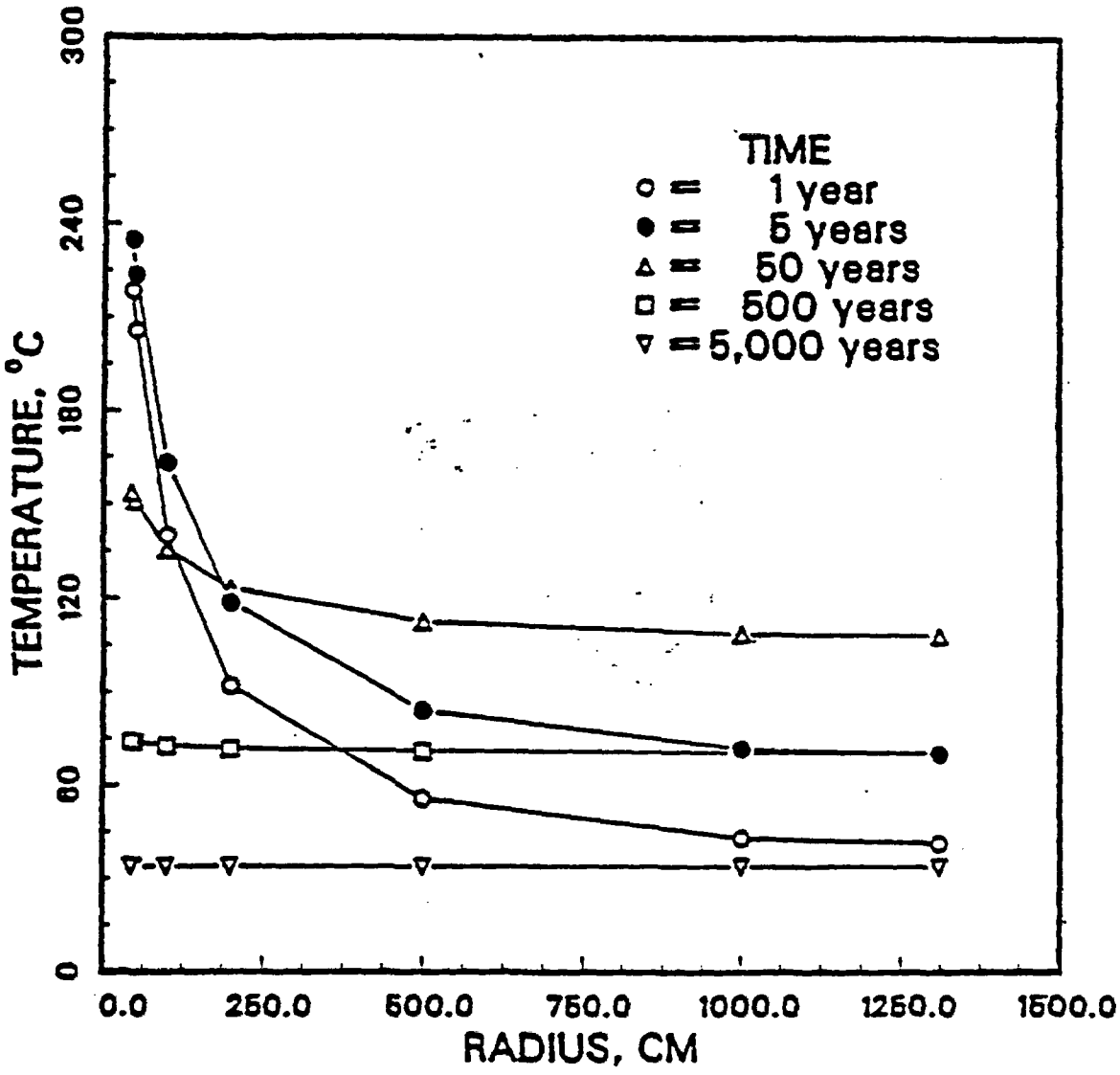

Figure 24 Temperature Profiles after Emplacement at Gibson Dome for CHLW

DA 2 4
DC 67

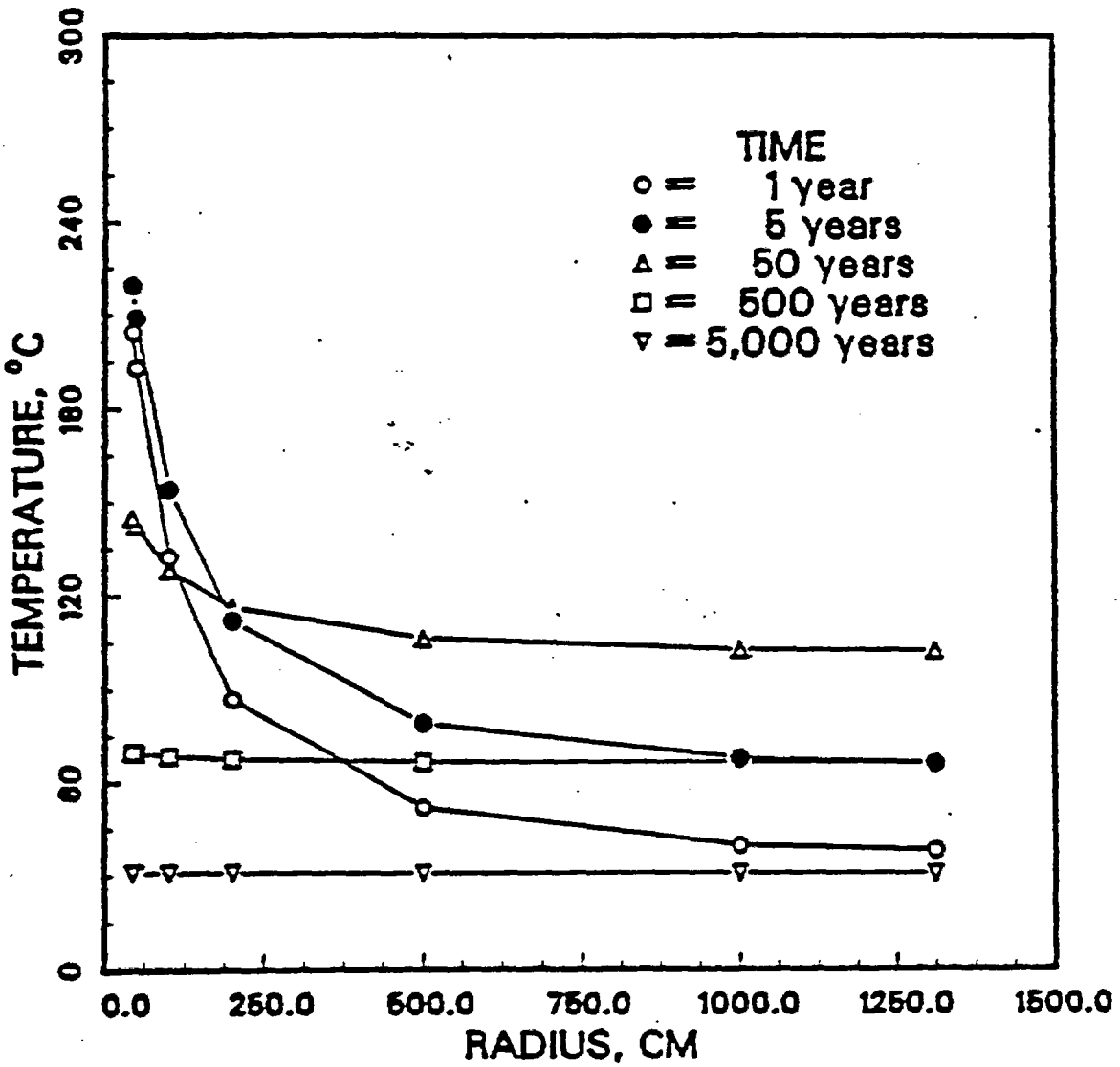

Figure 2.5 Temperature Profiles after Emplacement at Palo Duro for CHLW

PA24
DC68

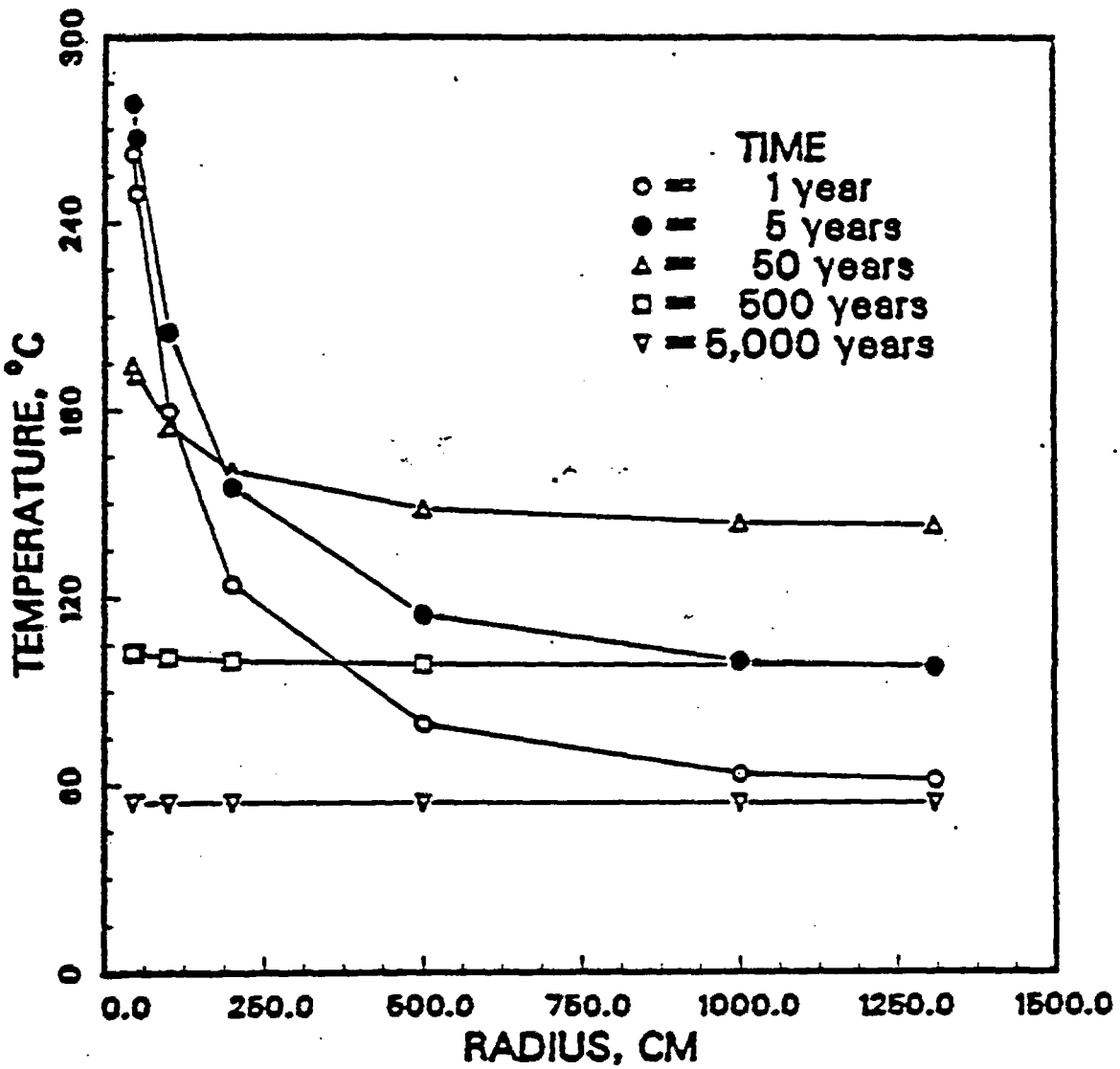

Figure 2b Temperature Profiles after Emplacement at Richton Dome for CHLW

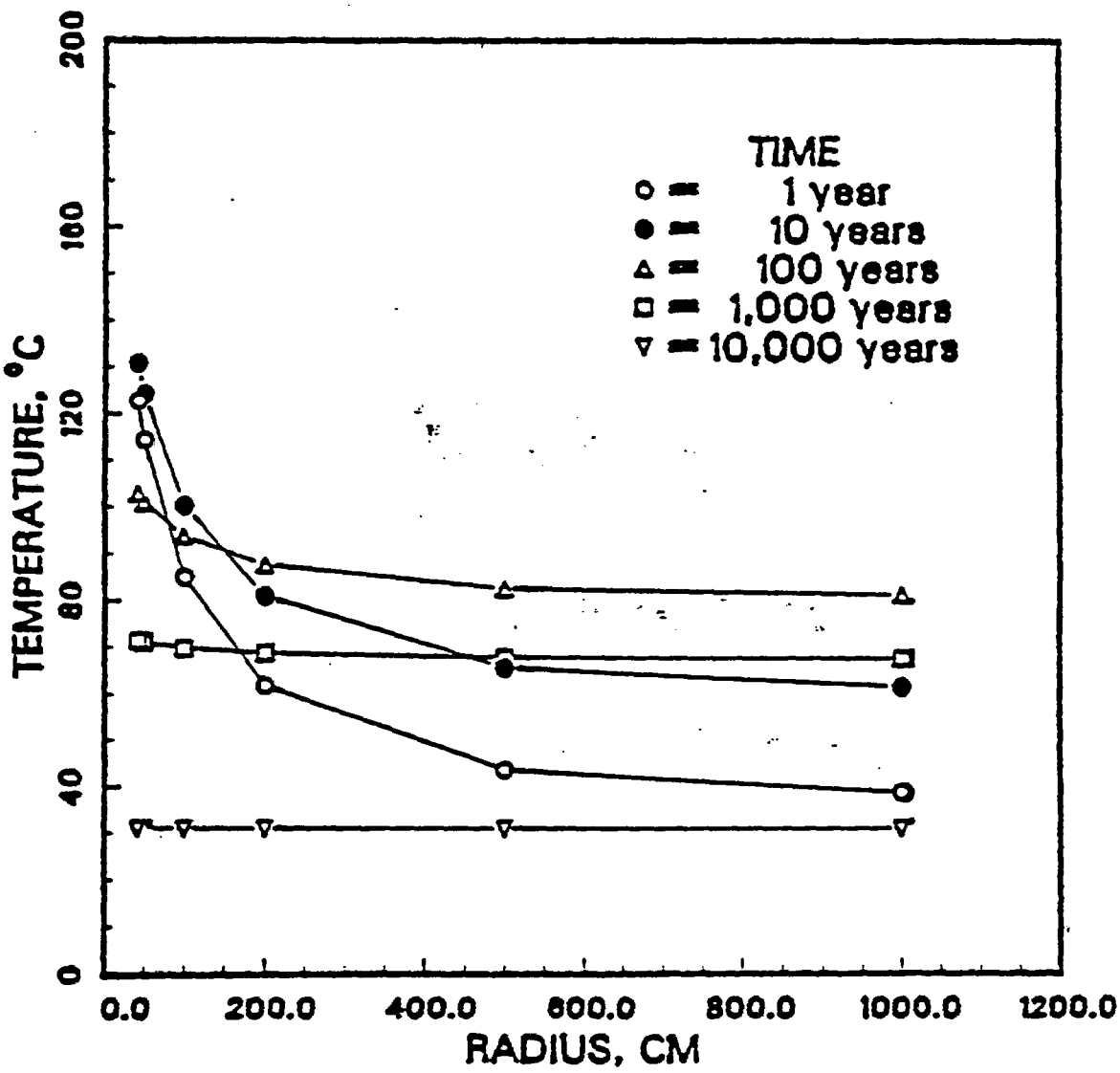

Figure 27 Temperature Profiles after Emplacement at Gibson Dome for SFPWR

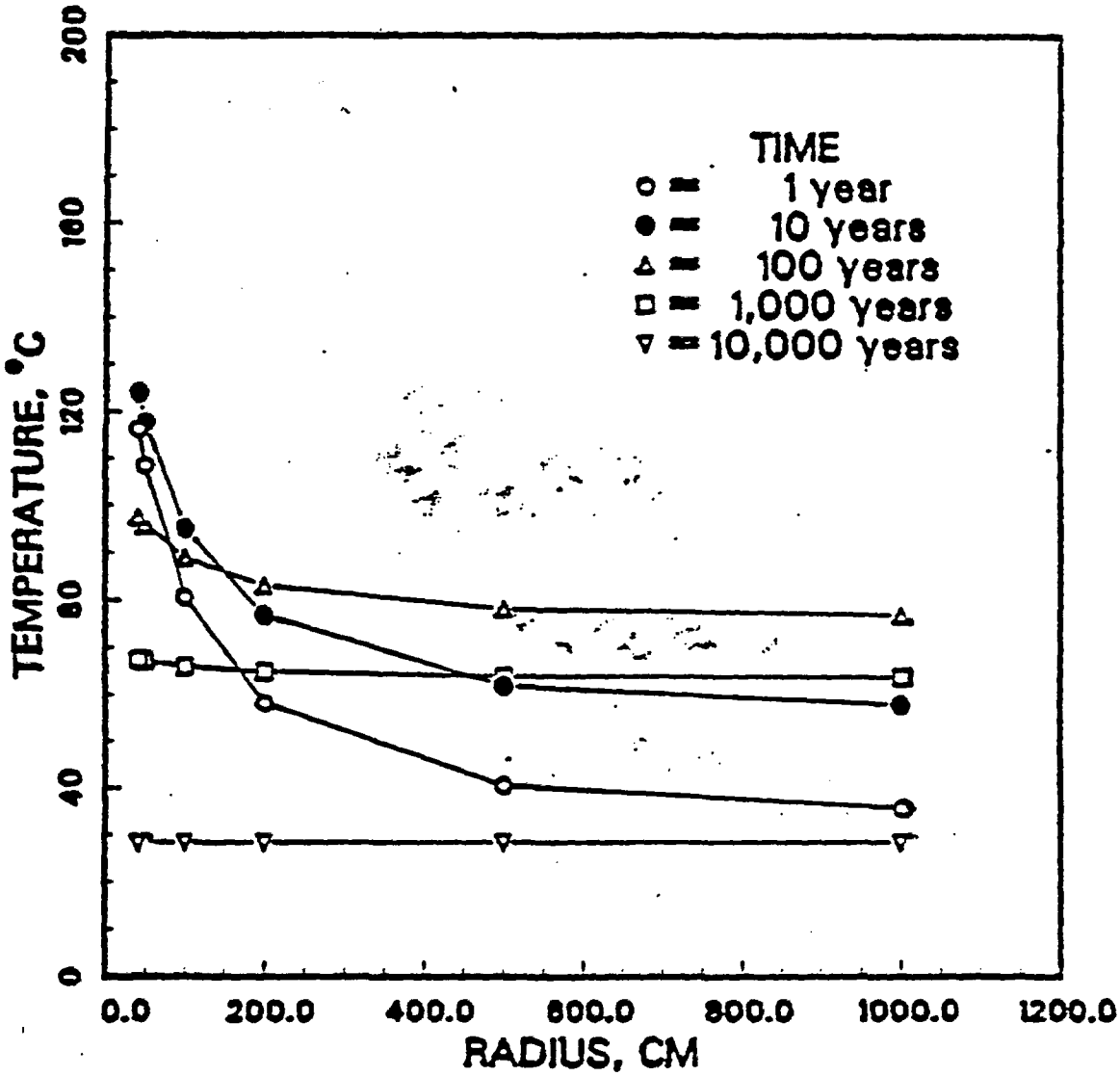

Figure 2.8 Temperature Profiles after Emplacement at Palo Duro for SFPWR

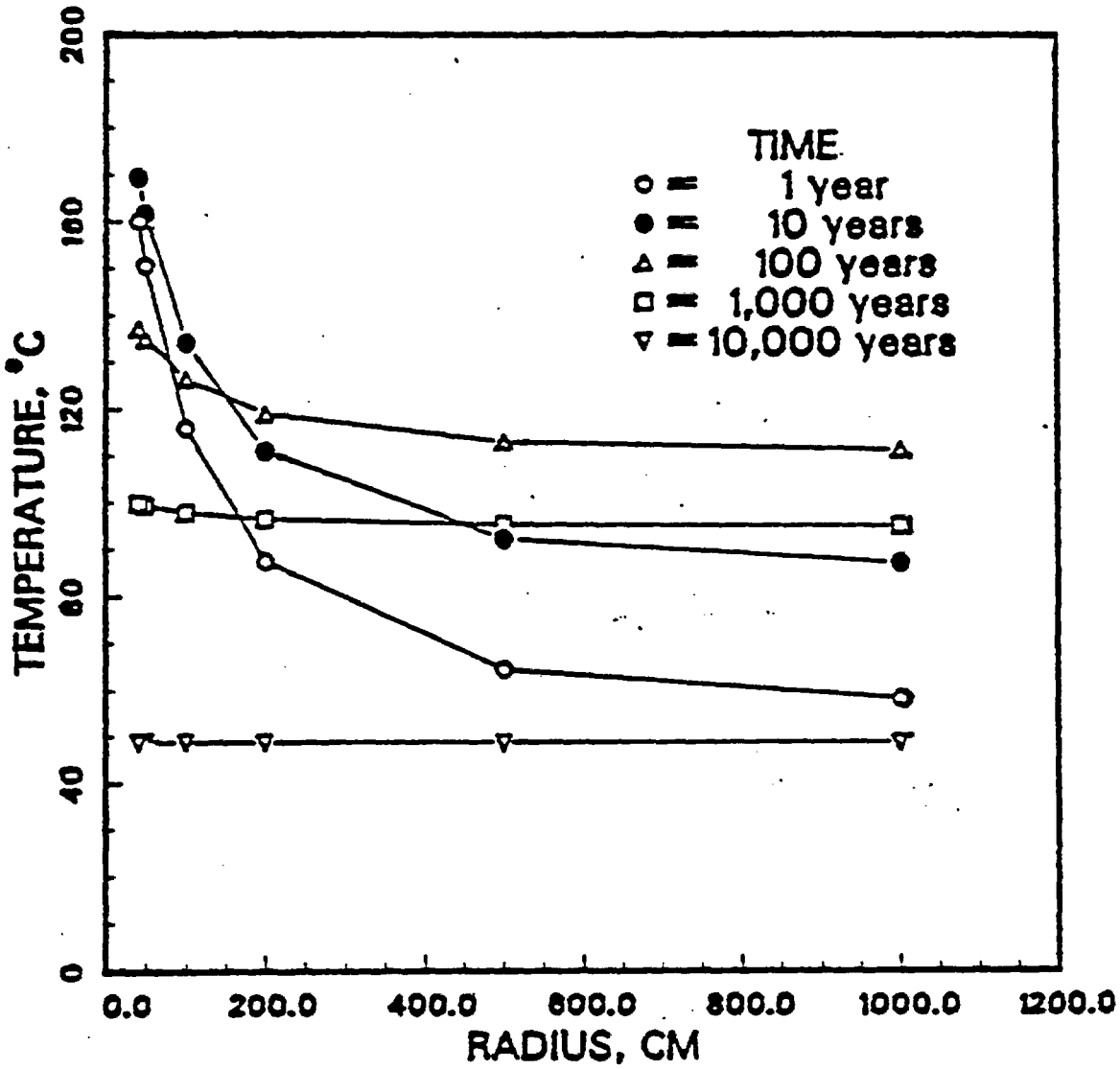

Figure 2.9 Temperature Profiles after Emplacement at Richton Dome for SFPWR

FA 2 H
DC 72

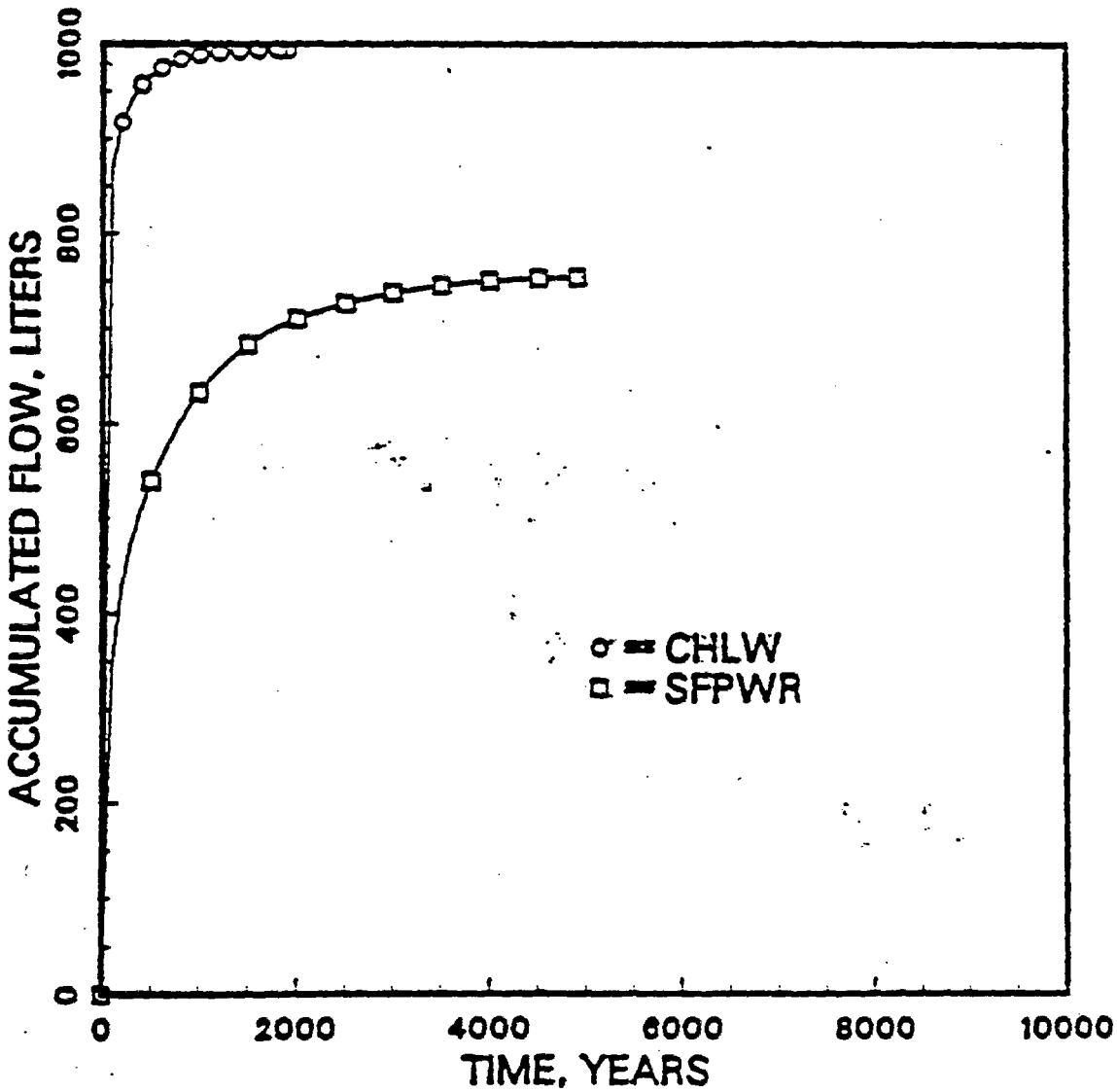

Figure 2.10 Accumulated Brine vs. Time for Gibson Dome, No Threshold Gradient

PA 2-4
DC 73

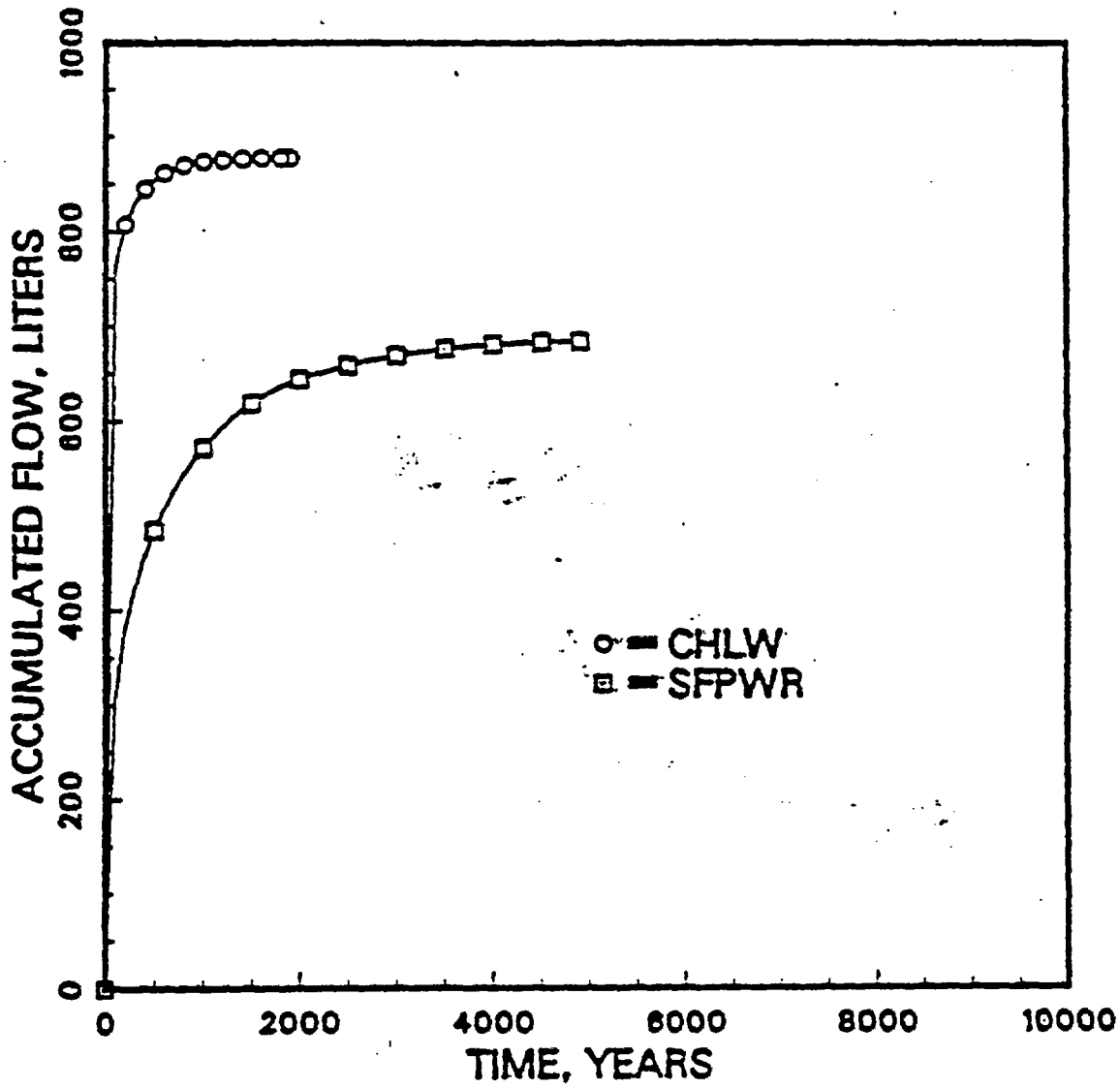

Figure 3.1 Accumulated Brine vs. Time for Palo Duro, No Threshold Gradient

DA 2 H
DC 70

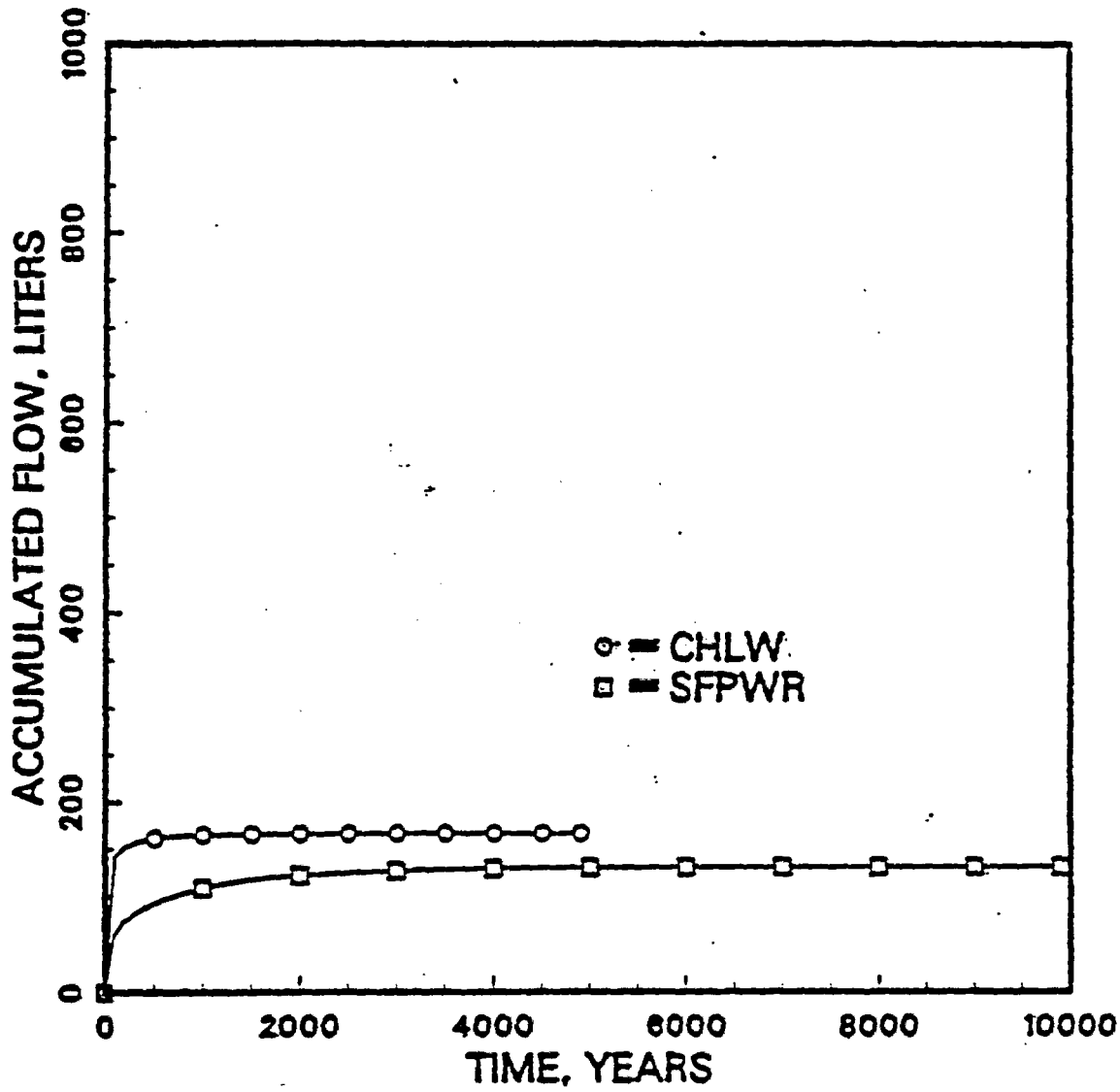

Figure 4.12 Accumulated Brine vs. Time for Richton Dome, No Threshold Gradient

PA 7H
DC - 75

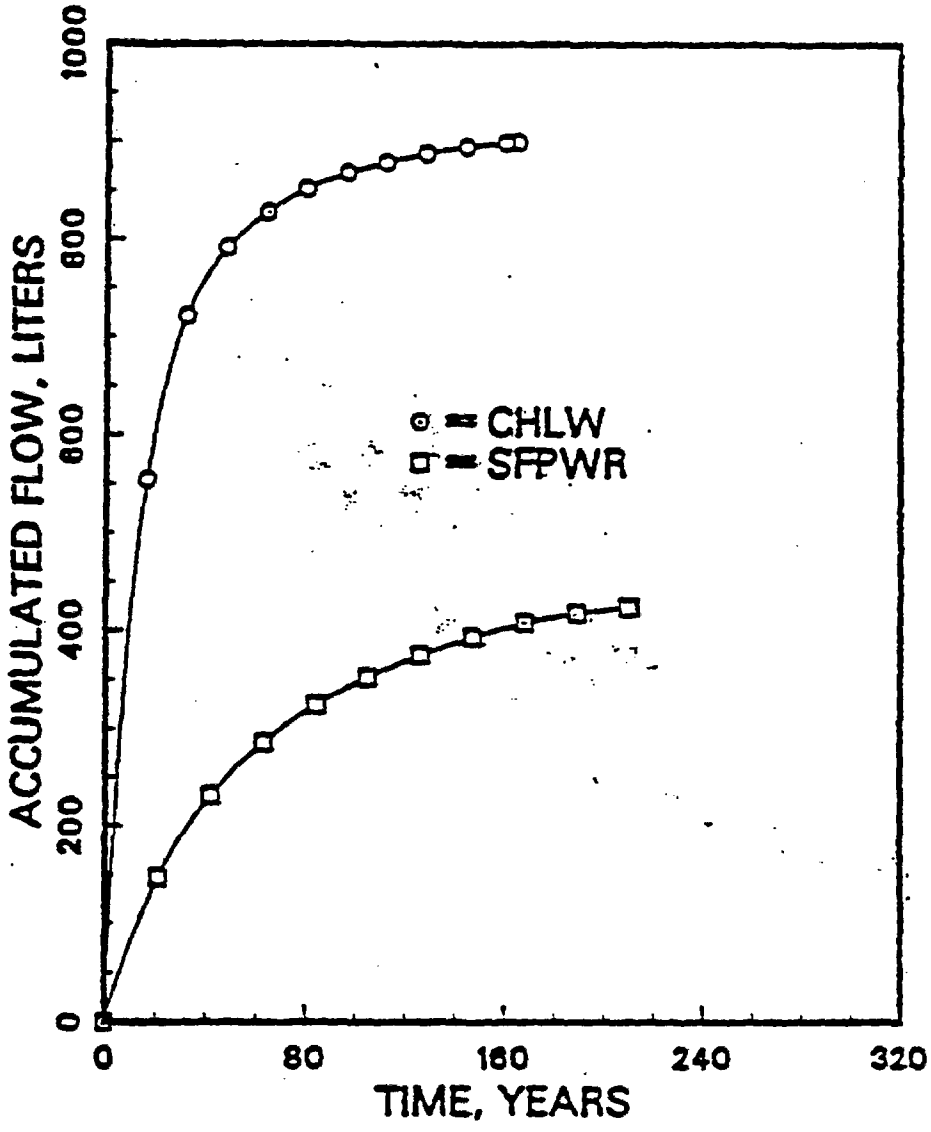

Figure 2.3 Accumulated Brine vs. Time for Gibson Dome, Threshold Gradient = 0.125 °C/cm

PA 2 4
DC 76

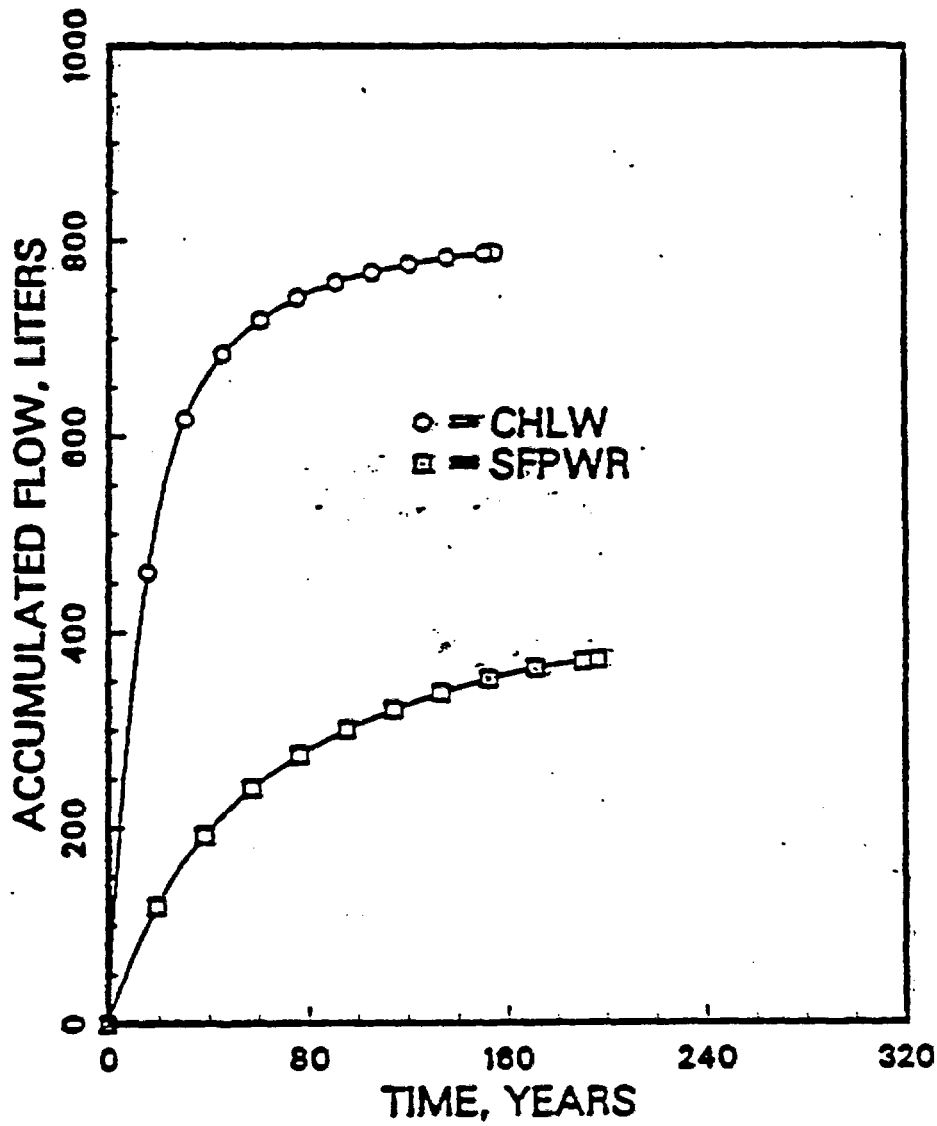

Figure 7.14 Accumulated Brine vs. Time for Palo Duro, Threshold Gradient = 0.125 °C/cm

DA2 H
DC 77

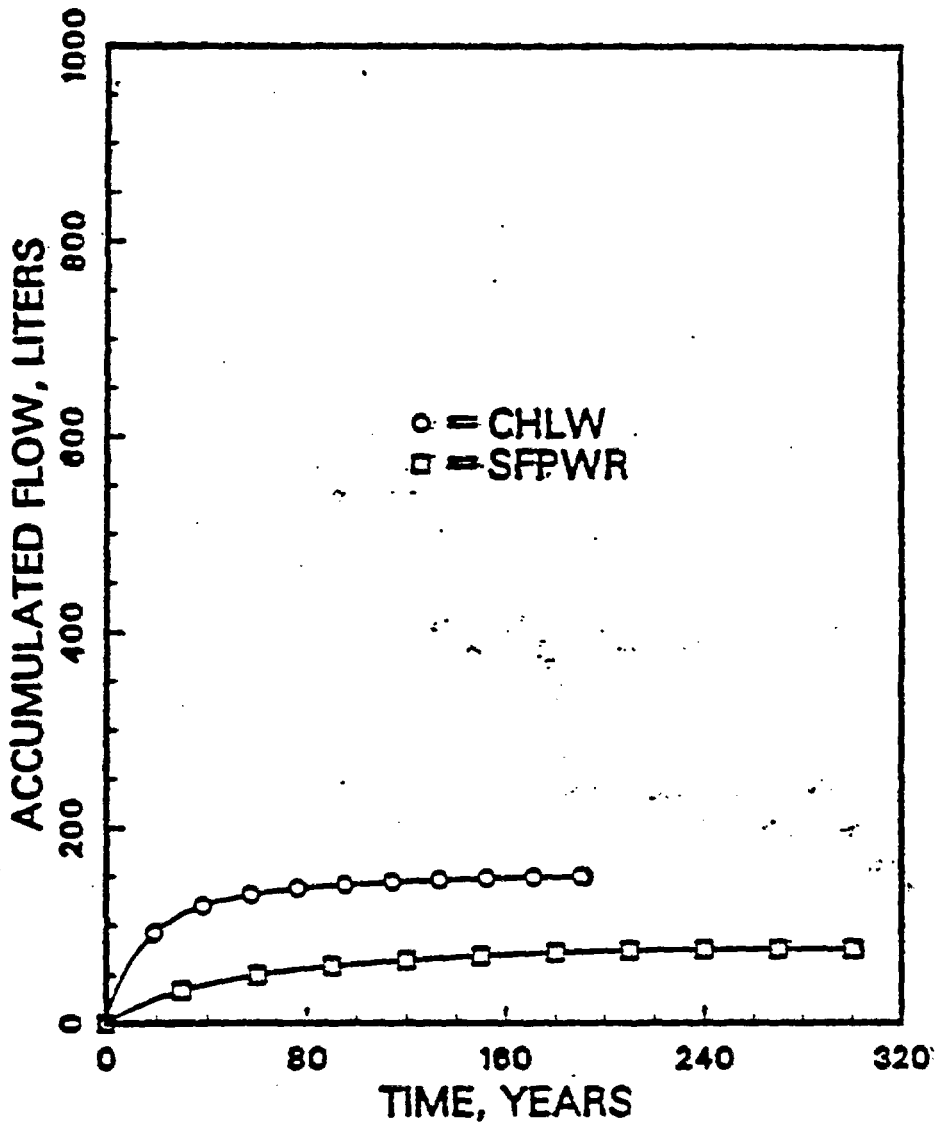

Figure 2.15 Accumulated Brine vs. Time for Richton Dome, Threshold Gradient = 0.125 °C/cm

PA 2-4
DC 78

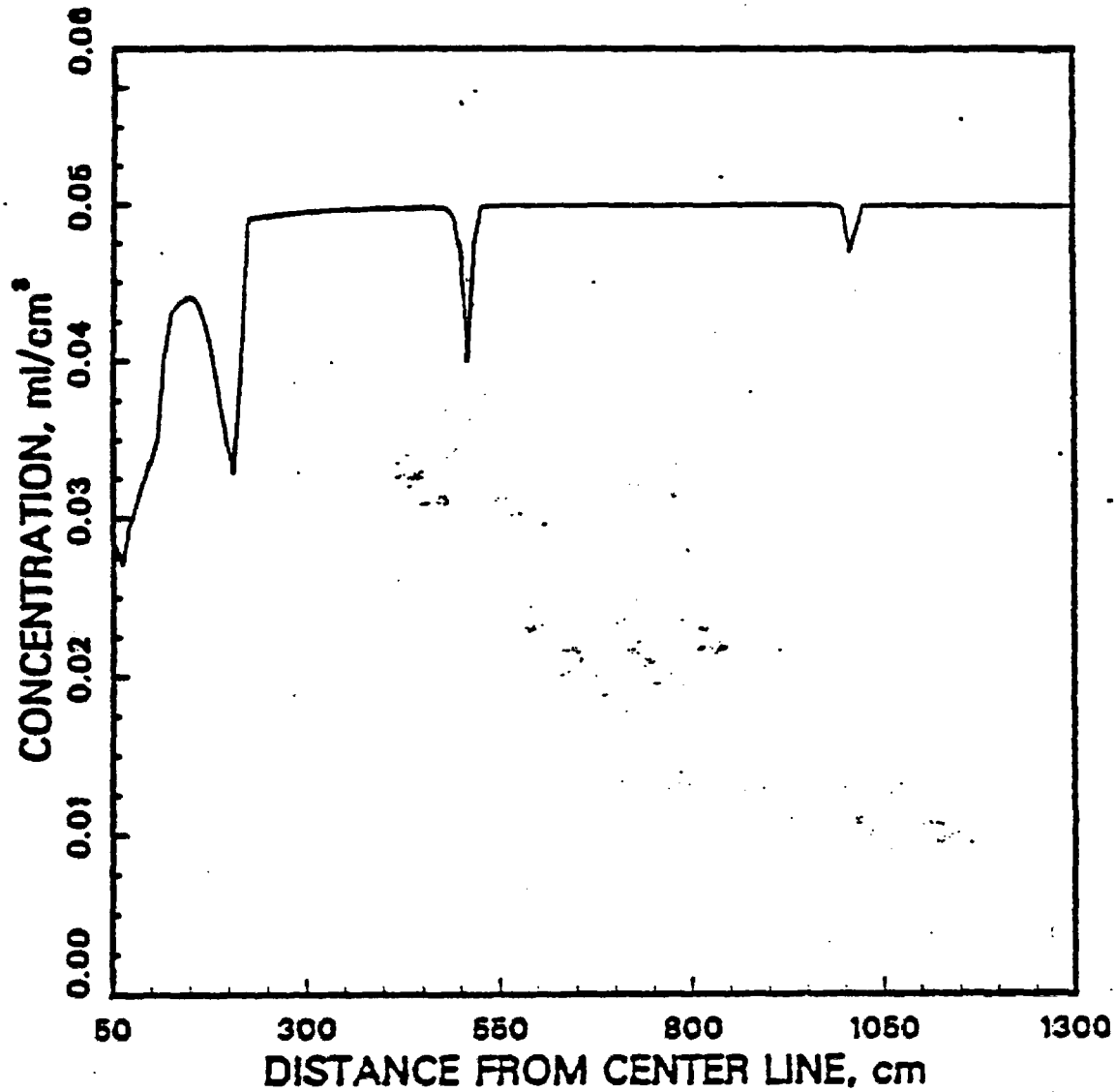

Figure 2.6 Final Concentration Profile at Gibson Dome for CHLW; No Threshold Gradient